PHARMACOLOGICAL AND IMMUNOLOGICAL CONTROL OF ZIKA VIRUS IN MICE DEFICIENT IN ADAPTIVE IMMUNE RESPONSES

Nathaniel Schramm

A thesis submitted to the faculty at the University of North Carolina at Chapel Hill in partial fulfillment of the requirements for the degree of Maters of Science in the Department of Microbiology and Immunology in the School of Medicine.

Chapel Hill
2019

Approved by:

J. Victor Garcia-Martinez

Ralph Baric

Myron Cohen

Raymond Pickles

ABSTRACT

Nathaniel Schramm: Pharmacological and immunological control of Zika virus replication in mice deficient in adaptive immune responses.
(Under the direction of J. Victor Garcia-Martinez)

Zika virus (ZIKV) has recently demonstrated epidemic potential with prolonged infection, sexual and mother to fetus transmission, severe clinical manifestation of fetal microcephaly and congenital malformations and Guillain-Barré syndrome in adults. Existing small animal models for ZIKV infection based on interferon (IFN)-deficient mice are not well suited for long-term assessment of therapeutics. Here, we show that in contrast to immunocompetent mice that control ZIKV infection and IFN-deficient mice that rapidly succumb to infection, immunodeficient mouse strains lacking T, B, and NK cells support systemic ZIKV replication for long periods of time. Using these immunodeficient mice, we evaluated the efficacy of 7-Deaza-7-fluoro-2'-C-methyl-adenoside (DFMA), a small molecular inhibitor and a neutralizing antibody (C10) to suppress systemic ZIKV replication in vivo. DFMA treatment resulted in efficient and sustained viral suppression. Treatment with C10 also resulted in viral suppression in highly clinically relevant tissues like the brain, eyes, gastrointestinal tract, and male and female reproductive organs.

For Becca.

ACKNOWLEDGMENTS

This work was supported by NIH grants AI106695 and AI125198 to R.S.B., and by NIH grant 1R21-AI-129607 and by the Emory University CFAR NIH grant 2P30-AI-050409 to R.F.S. The authors thank current and past members of the Garcia laboratory for technical assistance. We thank technicians at the UNC Division of Comparative Medicine. We acknowledge the editorial assistance and statistical consultation from Dr. Paul W. Stewart from the NC Translational and Clinical Sciences (NC TraCS) Institute, which is supported by the National Center for Advancing Translational Sciences (NCATS), National Institutes of Health, through Grant Award Number UL1TR002489. I would like to thank my mentor, J. Victor Garcia-Martinez, who steadfastly supported me through a turbulent graduate school career. I also extend my gratitude to Martina Kovarova, who provided scientific, writing, and professional guidance. Also, to Angela Wahl and the rest of the Garcia lab, and the Division of Comparative Medicine staff, without whose support I could not have reached this far. Also, I thank our primary collaborators for this work, the Baric lab and the Schinazi lab who provided the foundation for much of my work. Lastly, my utmost thanks to Orrin Thayer and Jenna Bone Honeycutt, who always made time to help me no matter their own schedules and made me develop my work ethic daily while teaching me the difference between just working in a lab and being part of something greater.

TABLE OF CONTENTS

LIST OF TABLES

LIST OF FIGURES

LIST OF ABBREVIATIONS

BM	Bone marrow
CVL	Cervical vaginal lavage
DENV	Dengue virus
DFMA	7-Deaza-7-fluoro-2'-C-methyl-adenoside
FRT	Female reproductive tract
IEL	Intraepithelial layer of the gastrointestinal tract
IFN	Interferon
IP	Intraperitoneal
IV	Intravenous
LPL	Lamina propria layer of the gastrointestinal tract
NOD/SCID	NOD.CB17-*Prkdc*^{scid}/J
NOG	NOD.Cg-*Prkdc*^{scid} *Il2rg*^{tm15ug}/JicTac
NSG	NOD.Cg-*Prkdc*^{scid} *Il2rg*^{trm1Wjl}/SzJ
ZIKV	Zika virus

CHAPTER 1: INVESTIGATING THE SUSCEPTIBILITY OF IMMUNE COMPETENT MOUSE MODELS TO ZIKA VIRUS INFECTION

Introduction

The flavivirus ZIKV envelope is highly dynamic and sensitive to pH changes, providing variable interaction sites with cellular receptors based on the degree of maturation of the virion (1, 2). This results in a large number of cell types being susceptible to ZIKV infection and wide tissue tropism (1, 3).

One of the most critical factors in replication of the ZIKV and production of mature virus particles is the pH changes from one intracellular compartment to the next. The structure of the ZIKV envelope protein, E, is particularly sensitive to changes in pH. After an endosome forms around the virus during cell entry, the low pH of 6.0 in the endosome causes structural rearrangements in the E glycoprotein, leading to the disassembly of the viral shell and fusion of the viral capsid (composed of C proteins) with the endosome (4). This fusion leads to the cytoplasmic release of the viral RNA (5).

The subgenomic ZIKV-RNA is then translated as a single polyprotein by cellular mechanisms. This polyprotein is cleaved into 3 structural (C, prM, and E) and 7 nonstructural proteins (NS1, NS2A, NS2B, NS3, NS4A, NS4B, and NS5) (6). The first of these cleavages is performed by NS3, which functions as a serine protease to auto-cleave the ZIKV polyprotein while associated with cofactor NS2B (7).

Genome replication, mRNA production, and initial assembly of the immature virion is initiated at the ER membrane (8). After cleavage, ZIKV NS1 localizes to the ER membrane, where it recruits additional non-structural proteins to assemble the replication factories typical of flaviviruses (9). At the ER membrane, NS4B induces formation of ER-derived membrane vesicles, where the NS5 RNA-dependent RNA-synthetase produces a dsRNA genome using the (+) sense ssRNA viral genome as a template (10). This dsRNA genome is then unwound by NS3 helicase (with cofactor NS4A) so that the genome can be transcribed into additional polyproteins by cellular machinery and replicated into (+) sense ssRNA genomes by NS5 (10). Another critical factor in the replication complex is NS2A (11).

Newly replicated (+) sense ssRNA genomes generated at the replication factories associated with the ER membrane will associate with capsid C protein and become enveloped by glycoproteins prM and E, along with cellular lipids from the ER membrane. ZIKV NS2A also plays a critical role here facilitating the incorporation of ER-derived membrane lipids into budding virions (11).

This culminates in budding of the immature virion into the ER. From there, the virion is transported to the *cis*-golgi along the secretory pathway. There, cellular furin cleaves prM into the pr peptide and the membrane protein M (12). Critically, this results in further structural rearrangement of the E protein as the virion approaches full maturation. Normally, the low pH (6.7 at *cis*-golgi – 6.0 at *trans*-golgi) in the golgi compartments would induce changes in the E protein leading to virion disassembly as happens in the endosome of a newly infected cell, but the pr peptide remains associated with the E protein at this low pH to prevent premature fusion (12). The secretory pathway continues and culminates in the release of the virion outside of the cell. Once outside of a golgi-derived vesicle, the higher pH outside of the cell allows for the dissociation of the pr peptide from the virion shell and the final maturation of the glycoprotein shell into a mature ZIKV protected by self-dimerized E proteins (12).

The flavivirus envelope maturation states have been well characterized in DENV, and a recent, comprehensive review proposes that based on sequence similarity and characterization, the ZIKV envelope shares these traits (1). Typically, the flavivirus particle is surrounded by M and E protein homodimers which are responsible for interacting with cell receptors for entry (13). However, prM cleavage is inefficient, resulting in a heterogeneic viral envelope (14). These viruses are still infection-competent, even when the shell is not in the fully matured state (1). In those cases, alternating conformations of the E proteins, the pr peptide, and the M protein can each be exposed for interacting with cell receptors (1). For example, a neutral pH ER during replication can cause final presentation of trimeric pr-M projections (2).

The resulting heterogeneic viral envelope causes highly variable tissue tropism. Some of the relevant cell receptors identified so far include C-type lectin receptors, which can be highly expressed in dendritic cells, monocytes, macrophages, and myeloid cells (15). ZIKV has also been demonstrated to be able to perform apoptotic mimicry to enter the cell (16). It has also been determined that binding affinity with the ZIKV E protein is low, so associations with multiple receptors is usually required before clatherin-

mediated endocytosis begins (16, 17). Of course, ZIKV has also been strongly linked to congenital malformation and Guillain-Barré syndrome as a result of its ability to directly infect neural progenitor cells and impair their proliferation (18). So, depending on which cell types are infected, different disease outcomes will be produced.

One chronic ZIKV-associated condition is microcephaly. ZIKV-associated microcephaly occurs with the highest incidence when mothers are infected with ZIKV during the first trimester of pregnancy (19). ZIKV is unique among flaviviruses in that it infects placental tissue and new virions are secreted from there directly into fetal capillaries, allowing access to the immune privileged fetal tissue (19). This trimester is when critical neural development would normally occur but can be impaired by ZIKV infection (20). One possible cause of the neurodevelopmental impairment is the ability of ZIKV NS2A to disrupt cortical neurogenesis via degradation of the adherens junction complex (18). A case study compiled using Brazilian patient data proposes that pregnant women infected with ZIKV are 8.6 times more likely to have a child who developed microcephaly compared to non-infected women (21).

In adults, ZIKV infection can sometimes lead to Guillain-Barré syndrome. Guillain-Barré is an autoimmune disorder which occurs infrequently in adults following infection or vaccination. However, South American case studies have reported higher incidence of Guillain-Barré syndrome during ZIKV epidemics, with increased severity and morbidity compared to patients who did not present with ZIKV infection, though the retroactive nature of the studies has made specific statistical estimates imprecise (22, 23). Although the precise mechanism of ZIKV-associated Guillain-Barré remains unidentified, it is likely related to the potential for ZIKV to broadly target C-type lectin receptors which are highly expressed in immune cells (15). Additionally, patients previously infected with DENV are at risk for an antibody dependent enhancement of ZIKV, which can greatly increase the risk of severe disease complications (24, 25).

Small animal models are critical to the study of disease pathology and the efficacy of novel therapies. I will expand on the nature and limitations of existing mouse models of Zika virus infection in the introduction to Chapter 2. Briefly, existing animal models of Zika virus infection have high mortality shortly after exposure, making them poor tools for studying chronic infection and long-term therapies (26,

27). We sought to characterize a mouse model with a Zika virus pathology that better mimics the nonlethal, persistent nature of human infection.

We began this study with immune competent BALB/c mice so that we could establish a baseline of ZIKV control in mice before working with immune deficient mouse strains. We found that although immune competent BALB/c mice very effectively control ZIKV infection in the periphery following intravenous exposure, viral-RNA was detected infrequently after exposure to the virus. Critically, low levels of ZIKV-RNA was detectable in multiple tissues analyzed from immune competent BALB/c mice harvested up to 329 days post exposure. Although immune competent BALB/c mice effectively clear ZIKV-RNA from the periphery shortly after exposure, we have found that the mice can maintain persistent infections which can result in peripheral ZIKV-RNA being detected in low quantities.

Results

Immune competent BALB/c mice maintain detectable levels of Zika virus RNA in multiple tissues up to six months post exposure. Due to the capacity for mouse IFN to effectively restrict ZIKV, the virus is rapidly cleared in the periphery of immune competent mice. We exposed a group of male BALB/c mice (n=18) intravenously to H/PF/2013 (5.0×10^5 FFU).

At one, three, and six months post exposure, tissues were harvested from six mice. The tissues we assessed for localized ZIKV-RNA from each mouse were lung, liver, spleen, bone marrow, brain, intraepithelial layer of the gastrointestinal tract (IEL), lamina propria layer of the gastrointestinal tract (LPL), eye, prostate, epididymis, seminal vesicles, prostate, penis, and testes (Table 1.1) At one month post exposure, low levels of ZIKV-RNA were detected in 4/6 mice. Virus was found in 3/6 spleens, 2/6 testes (analyzed in pairs), and 1/12 eyes (two from each mouse, analyzed individually). The highest viral RNA levels recorded at this time was in the spleen of one of the mice, which had 36 copies of ZIKV-RNA per 10^5 cells. Three months post exposure, we did not detect ZIKV-RNA in any of the tissues tested. Of the six animals randomly selected for necropsy at this time point, only one had detectable ZIKV-RNA in the periphery after 2 days post exposure, so the relative reduction in tissue resident ZIKV-RNA is not totally unexpected (Figure 1.1, Table 1.1). We were able to detect peripheral ZIKV-RNA more frequently between three and six months post exposure (Figure 1.1). This resulted in a greatly increased frequency of detectable ZIKV-RNA in all tissues tested at six months post exposure (Table 1.1). ZIKV-RNA was detectable in at least one tissue of all six mice analyzed and was most consistently detected in testes and liver (6/6 mice). It was also detected in the seminal vesicles of one mouse. The most viral RNA we detected at this time point was 1.3×10^3 copies ZIKV-RNA/10^5 cells in the testes of one mouse.

In the periphery, the viral load was $8.1 \times 10^4 \pm 1.2 \times 10^4$ s.e.m. ZIKV-RNA copies/mL plasma two days post exposure (Figure 1.1). By five days post exposure, ZIKV-RNA was undetectable in the periphery of all 18 animals (Figure 1.1). At 56 days post exposure, 2/12 remaining animals had detectable ZIKV-RNA (586 and 764 copies/mL plasma). After 100 days post exposure, low-quantity ZIKV-RNA became more frequent in the plasma of the six remaining mice (Figure 1.1). Of the 18 mice, none developed observable physical or neurological symptoms of ZIKV infection during the period of

experimentation. Despite rapid peripheral control of ZIKV infection in immune competent BALB/c mice, persistent infection was maintained in some of the animals up to six months post exposure.

BALB/c mice do not completely clear ZIKV-RNA from the periphery when CD4+ and CD8+ T cells are depleted. Given the presence of neurological symptoms suggestive of encephalitis in the intranasally exposed mice and the presence of detectable viremia long after exposure in intravenously exposed mice, we were very interested in the role that adaptive immune cells play in fighting ZIKV infection in BALB/c animals. To investigate the role of the adaptive immune system in BALB/c mice, we depleted $CD4^+$ and $CD8^+$ T cells prior to intravenous exposure (5.0×10^5 FFU) with ZIKV H/PF/2013 (n=6). This depletion was maintained through the course of the experiment and regularly confirmed via flow cytometry of peripheral blood. Two days post exposure, the peripheral viral load in the six animals tested was $5.9 \times 10^3 \pm 5.3 \times 10^2$ s.e.m. ZIKV-RNA copies/mL plasma compared to $8.1 \times 10^4 \pm 1.2 \times 10^4$ s.e.m. ZIKV-RNA copies/mL plasma in undepleted controls (p=0.0034 Mann-Whitney test) (Figure 1.1, Figure 1.2). Importantly, all six of the animals tested had detectable ZIKV-RNA in the periphery during the course of the experiment (91 days total) which presented as transient, low-quantity detectable viremia (Figure 1.2). This is in direct contrast to the undepleted controls (0-1 month: n=18, 1-3 months: n=12, 3-6 months: n=6), which presented only two instances of detectable viremia through 106 days post exposure (Figure 1.1).

One possible cause for this reduction in viral load with an increased frequency of detectable viremia in an immune compromised mouse is the demonstrated capacity for ZIKV to infect lymphocytes. By depleting $CD4^+$ and $CD8^+$ T cells, ZIKV was able to establish a somewhat more productive infection but fewer targets of peripheral infection were provided during the initial exposure, resulting in less peripheral virus at two days post exposure compared to undepleted controls but more frequent instances of detectable viremia as the experiment progressed (Figure 1.1, Figure 1.2).

Analysis of replication and long-term persistence of ZIKV in immune competent mice. Long-term persistence of ZIKV after peripheral clearance has not been adequately described. After considering the frequently detectable virus in our six month post exposure harvests (Table 1.1) and the impact of $CD4^+$ and $CD8^+$ T cell depletion on peripheral virus (Figure 1.2), we designed an experiment that would examine the capacity of ZIKV to rebound in immune competent mice long after initial

peripheral clearance and depletion of $CD4^+$ and $CD8^+$ T cells. To evaluate ZIKV persistence in immune competent mice, a group of BALB/c mice (n=10) were intravenously exposed to 5.0×10^5 FFU ZIKV H/PF/2013 (Figure 1.3A). Two days after exposure, ZIKV-RNA was detected in all animals (mean viral load of $4.9 \times 10^3 \pm 3.2 \times 10^3$ s.e.m. ZIKV-RNA copies/mL plasma) (Figure 1.3B). By ten days post exposure, ZIKV-RNA was undetectable in the plasma of all animals. Plasma was monitored weekly for the first month after infection, and no viral rebound was detected. The mice were analyzed again at 201 and 283 days post exposure to confirm long-term suppression of viremia. Two male mice were found dead in their cage 130 and 268 days post exposure. Neither animal had evidence of ZIKV in plasma at the last timepoints analyzed and tissues could not be examined. To investigate the possible role of adaptive immune cell-mediated control of viral replication, starting 287 days post exposure, $CD4^+$ and $CD8^+$ T cells were depleted from these animals for 42 days (Figure 1.3A). $CD4^+$ and $CD8^+$ T cell depletion was confirmed in peripheral blood by flow cytometry (Figure 1.3C, left). Despite effective depletion of both $CD4^+$ and $CD8^+$ T cells, no viral rebound was detected in the periphery. Finally, at 329 days post ZIKV exposure (42 days after $CD4^+$ and $CD8^+$ T cell depletion), necropsy was performed and flow cytometric analysis of splenocytes was used to demonstrate efficient tissue $CD4^+$ and $CD8^+$ T cell depletion (Figure 1.3C bottom right). In addition, tissues where high ZIKV replication levels are observed in macaques or in humans were collected from the mice for real-time PCR analysis of localized viral persistence (brain, epididymis, testes or female reproductive tract [FRT] and eyes). No ZIKV-RNA was detected in any of the samples analyzed from spleen, brain, epididymis, testes or the FRT (Figure 1.3D). However, several hundred copies of ZIKV-RNA were detected in eyes from two mice. Our results demonstrate that despite efficient control and clearance in the periphery, in some animals ZIKV-RNA can persist in the eyes for almost a year post exposure.

Immune competent BALB/c mice lose coordination and balance following intranasal ZIKV exposure. We performed intranasal exposures (1.0×10^6 FFU ZIKV H/PF/2013) of immune competent BALB/c mice (n=4 with n=4 vehicle controls). The method of intranasal exposure we performed was chosen because it preferentially infects the brain in mice through the palate and sinuses. Two days after exposure, ZIKV-RNA was detectable in 3/4 BALB/c mice (666 ± 217 s.e.m. copies/mL plasma)(Figure 1.4A). By five days post exposure, ZIKV-RNA was detectable in 4/4 BALB/c mice ($1.1 \times 10^3 \pm 4.2 \times 10^2$

s.e.m. copies/mL plasma). At the last time point evaluated, only 2/4 BALB/c mice had detectable ZIKV-RNA ($2.5 \times 10^4 \pm 1.6 \times 10^4$ s.e.m. copies/mL plasma), though it did increase ten-fold in the mice where it remained detectable.

Mice were scored for neurological symptoms each day for a period of nine days after exposure: 1 – loss of balance/ataxia; 2 – hind-limb paralysis with forelimb clutching; 3 – hind-limb paralysis with forelimb weakness; 4 – limb paralysis and difficulty eating and drinking. Critically, loss of balance and coordination was detected in the ZIKV-exposed BALB/c animals starting three days post exposure (Figure 1.4B). Three- and four-days post exposure, loss of balance was recorded in 3/4 BALB/c mice and in 4/4 BALB/c mice from five days post exposure until the end of the experiment. The presence of neurological symptoms in the immune competent mice point to the possibility of encephalitis induced neurological symptoms following ZIKV infection.

Discussion

The existence of infected reservoirs was reported in flavivirus infection before the recent ZIKV epidemic. Specifically, it has been reported in brain and nervous tissue up to 10 years after Siberian Tick Borne Encephalitis virus infection, in cerebrospinal fluid three weeks after infection and in PBMCs 8 months after infection with Japanese Encephalitis virus, and in donated tissue 40 days after infection and in urine six-and-a-half years after infection with West Nile virus (28-30). However, persistent ZIKV infection has a larger impact on public health because of the capacity for ZIKV to be sexually transmitted long after recovery from disease symptoms (31). ZIKV reservoirs have been confirmed in human eyes, testes, placenta, nervous tissue, and kidneys, with persistent shedding identified in vaginal secretions, urine, and semen (28, 31-37). These findings reinforce the need for a ZIKV animal model that can recapitulate human infection on an appropriate time scale.

In immune competent mice, the inability of NS5 to inhibit murine STAT2 results in a strong type I IFN response, suppression of virus replication and control of ZIKV infection (38, 39). This is consistent with our results in BALB/c mice intravenously exposed to ZIKV H/PF/2013. We determined that ZIKV can establish a persistent infection in immune competent BALB/c mice up to one-year post exposure despite initial clearance from the periphery after five days post exposure and no signs of illness at any point after infection. Critically, virus was detectable in critical tissues such as the brain, eyes, and male genital tract six months post exposure. Given the growing concern that persistent infection could magnify the risk of horizontal transmission in humans, long after the virus was believed to be cleared, a mouse model recapitulating this is of great importance (28). These findings highlight the lack of a ZIKV model for persistent infection on this time scale (28).

Depletion of mouse T cells 287-329 days after exposure did not result in peripheral rebound of viremia supporting the importance of the innate immune response to ZIKV control in mice. However, 2/8 mice were positive for ZIKV-RNA almost a year post-exposure. Other research groups have found that ZIKV infects cornea, iris, optic nerve, ganglion and bipolar cells in the retina and that it can persist in the eye through the convalescent stage possibly resulting in retinitis, focal retinal degeneration, and ganglion cell loss (40, 41).

ZIKV-associated fetal microcephaly is a direct result of ZIKV infecting the brain and central nervous system (18, 19, 21). The capacity for ZIKV to establish infection in immune privileged tissues such as the testis, brain, and placenta, is well established, but infection of adult human nervous tissue is not thoroughly characterized (28). Commonly used mouse models of ZIKV infection demonstrate neurological symptoms such as limb paralysis and dragging (26). In our experiments, the intranasally exposed BALB/c mice developed ataxia, a symptom of encephalitis, just a few short days after exposure. All of the immune competent mice we tested showed loss of coordination and balance through the experiment, even when virus was not detectable in the plasma. Future experiments in this study have the potential to demonstrate large scale lymphocyte migration to the brain.

Chapter 2, an adapted manuscript draft, will expand greatly on this work by more completely characterizing the unique pathology of the Zika virus in NSG mice and by taking advantage of its long survival to test novel therapeutics.

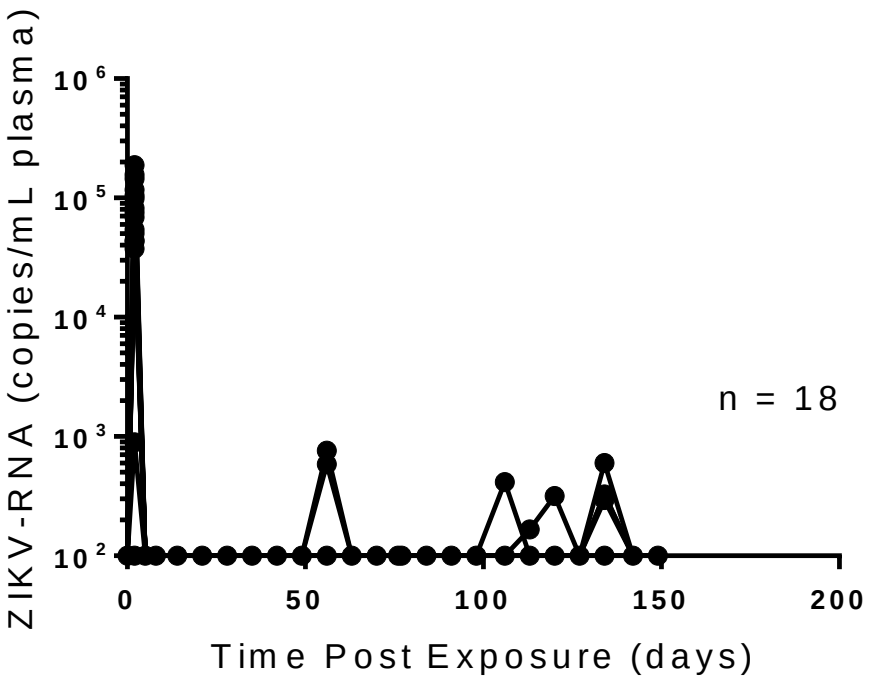

Figure 1.1. ZIKV-RNA in plasma from BALB/c mice. Analysis of ZIKV-RNA in plasma of infected BALB/c mice (n=18 mice). Mice were intravenously exposed to ZIKV H/PF/2013 (5.0 x 10^5 FFU). Six mice were harvested at one and three months post exposure to perform in depth tissue analysis. Values were calculated from a standard curve.

Table 1.1. Analysis of ZIKV-RNA in tissues from immune competent BALB/*c* mice up to one year post exposure.

	1 Month	3 Month	6 Month	1 Year
Lung	0/6	0/6	4/6	NA
Liver	0/6	0/6	6/6	NA
Spleen	3/6	0/6	5/6	0/8
Bone Marrow	0/6	0/6	4/6	NA
Brain	0/6	0/6	4/6	0/8
IEL	0/6	0/6	4/6	NA
LPL	0/6	0/6	4/6	NA
Eye	1/12	0/12	7/12	2/8
Prostate	0/6	0/6	4/6	NA
Epididymis	0/6	0/6	5/6	0/3
Seminal Vesicles	0/6	0/6	1/6	NA
Penis	0/6	0/6	5/6	NA
Testes	2/6	0/6	6/6	0/3
FRT	NA	NA	NA	0/5

NA – Not assessed

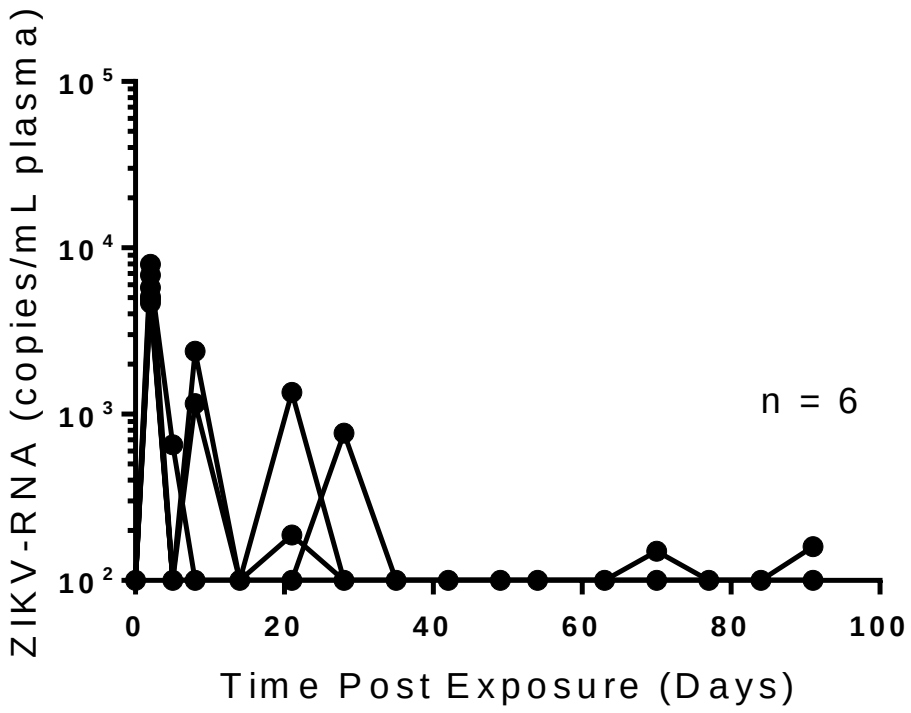

Figure 1.2. ZIKV-RNA in periphery of CD4 and CD8 T cell depleted BALB/c mice. Analysis of ZIKV-RNA in plasma from infected BALB/c mice (n=6 mice). Mice were intravenously exposed to ZIKV H/PF/2013 (5.0 x 10^5 FFU). Mice were depleted of $CD4^+$ and $CD8^+$ T cells before exposure and through the course of the experiment using anti-mCD4 (GK1.5) and anti-mCD8 (2.43) antibody treatment. $CD4^+$ and $CD8^+$ T cell depletion was confirmed regularly by flow cytometry analysis of peripheral blood. Values were calculated using a standard curve.

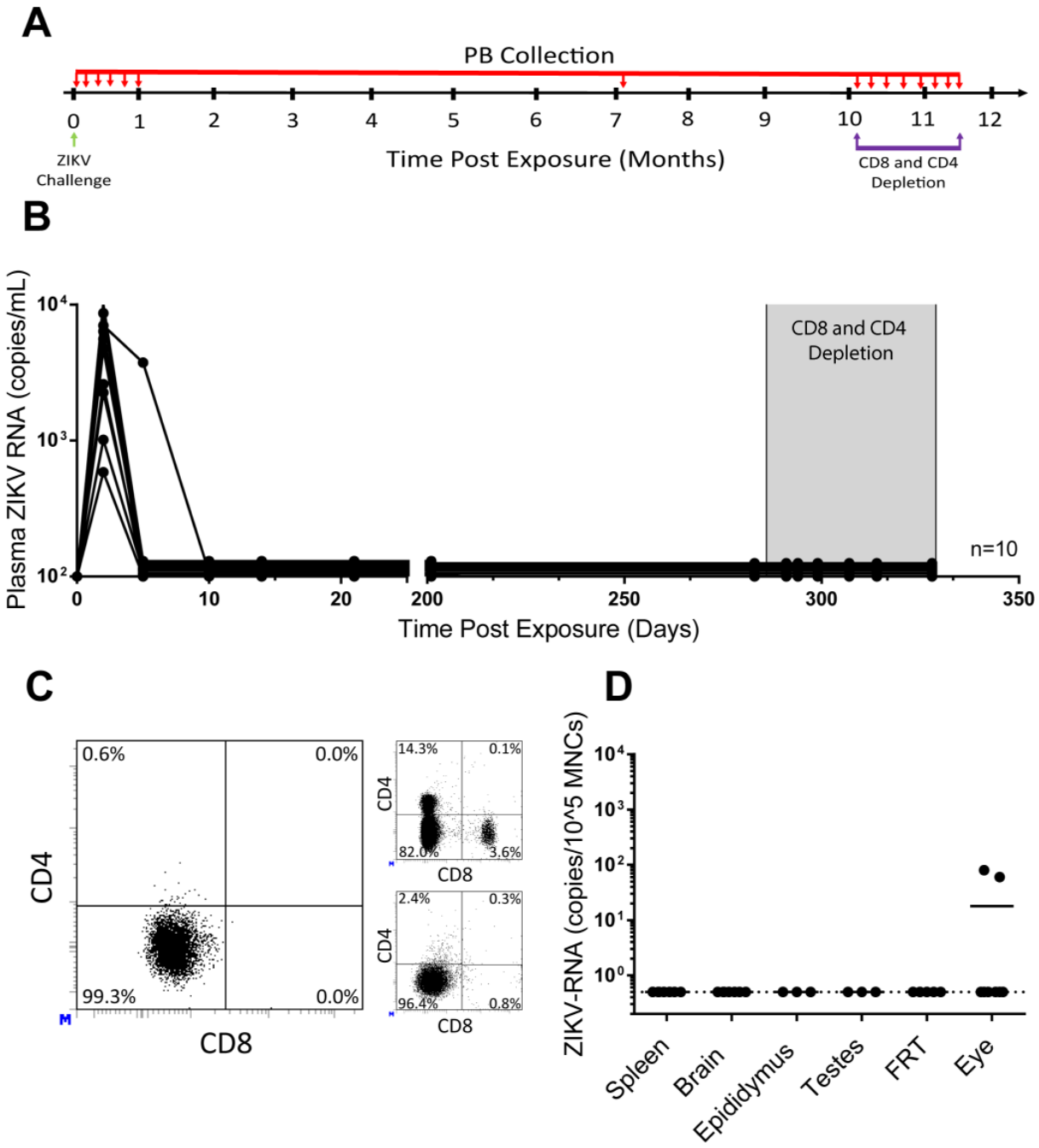

Figure 1.3. Control of ZIKV replication and persistence in BALB/c mice. (A) Experimental design. BALB/c mice (5 males and 5 females) intravenously exposed to ZIKV H/PF/2013 (5.0 x 10^5 FFU) were monitored over time for the presence of ZIKV-RNA in peripheral blood (PB, small red arrows). Mice were depleted of $CD4^+$ and $CD8^+$ T cells at 286 days post-exposure using anti-$mCD4^+$ (GK1.5) and anti-$mCD8^+$ (2.43) antibody treatment. Cell-associated ZIKV-RNA levels in multiple tissues were analyzed after 42 days of T-cell depletion. (B) Analysis of ZIKV-RNA in plasma of infected BALB/c mice (n=10 mice).

Shaded area represents the period of antibody treatment. (C) Flow cytometric analysis of peripheral blood confirming $CD4^+$ and $CD8^+$ T cell depletion in ZIKV-infected BALB/c mice after treatment with anti-T cell depleting antibodies. Flow cytometric analysis showing the presence of T cells in untreated mice (top right) and demonstrating efficient depletion of splenocytes at the time of harvest (bottom right) are included. Samples for flow cytometry analysis were gated as follows: singlets → live cells → $mCD45^+$. (D) ZIKV-RNA levels in tissues of BALB/c mice harvested 329 days post-exposure and 42 days after $CD4^+$ and $CD8^+$ T cell depletion (spleen, brain, eye, n = 8. Epididymis, testes, n = 3. Female reproductive tract n = 5). Samples without detectable ZIKV-RNA are placed on the dashed line. Horizontal line showing the mean MNC = mononuclear cells.

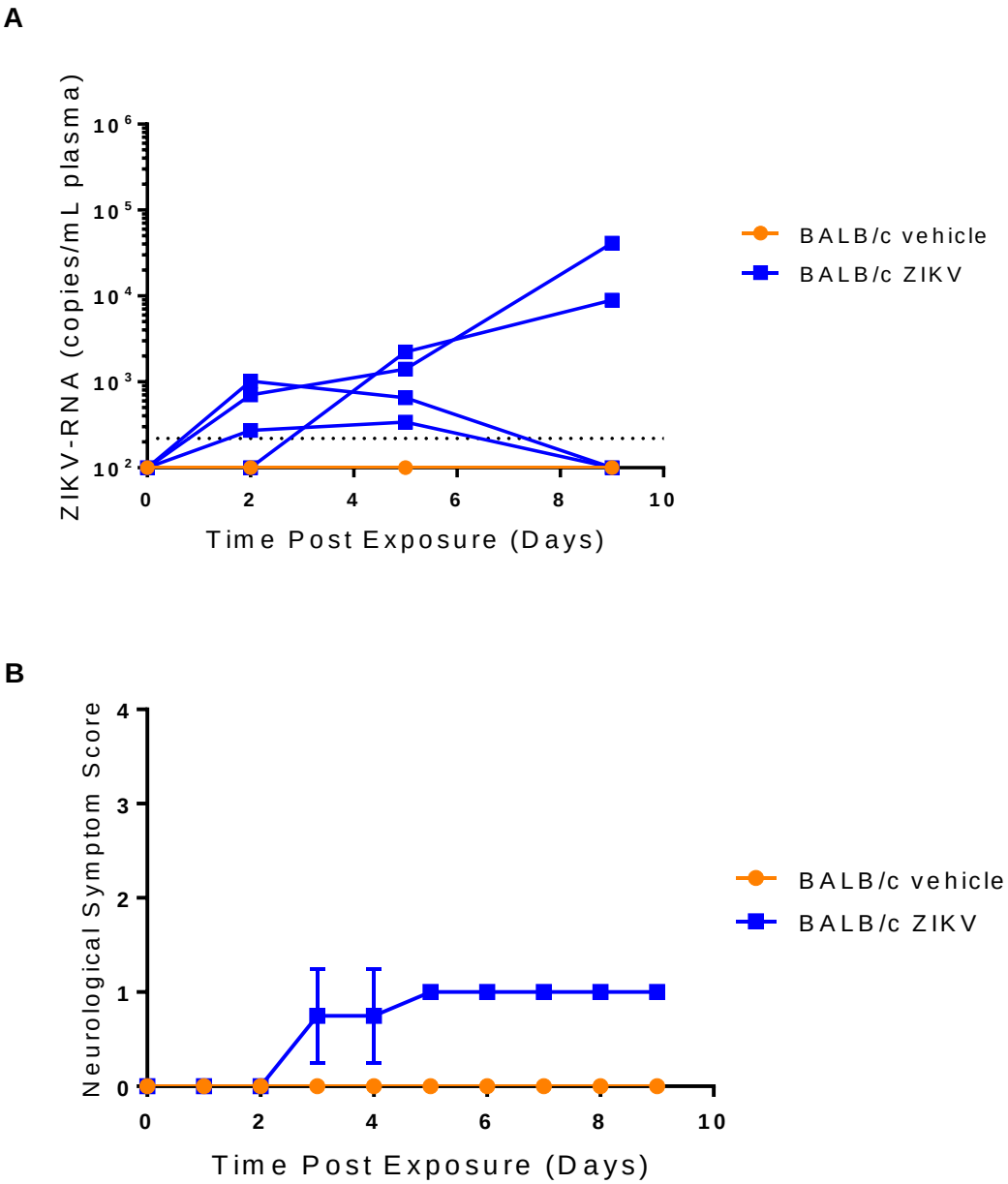

Figure 1.4. Intranasal exposure to ZIKV induces neurological symptoms in immune competent BALB/c mice but not immune deficient NSG mice. (A) Analysis of ZIKV-RNA in plasma of ZIKV exposed and vehicle control inoculated BALB/c (n=4 for each group). Mice were intranasally exposed to ZIKV H/PF/2013 (1.0 x 10^6 FFU). Values were calculated using a standard curve.

(B) The mice were scored for neurological symptoms each day following intranasal exposure. Scoring: 1 – loss of balance/ataxia; 2 – hind-limb paralysis with forelimb clutching; 3 – hind-limb paralysis with forelimb weakness; 4 – limb paralysis and difficulty eating and drinking.

Methods

Mice

BALB/c and immunodeficient NOD/SCID/$\gamma c^{-/-}$ (NSG) mice were used for experiments at 12-20 weeks of age. Mice were maintained by the Division of Comparative Medicine at UNC-Chapel Hill according to protocol approved by the Institutional Animal Care and Use Committee.

Virus challenges

Stocks of ZIKV H/PF/2013 were prepared as previously described (50). Viral challenges were performed by diluting viral stocks in RPMI (Gibco, Gaithersburg, MD). Virus (300 FFU – 2.5 x 10^5 FFU) was administered intravenously via tail vein injection (200 µL volume). Virus (1.0 x 10^6 FFU) for intranasal challenge was delivered via micropipette directly into the nostrils (20 µL volume) while the mouse was held upside down.

Collection and processing of mouse bodily fluids

Mouse peripheral blood was collected longitudinally for ZIKV-RNA quantification. Peripheral blood was collected into tubes containing anti-coagulant (EDTA solution, Sigma-Aldrich, St. Louis, MD). Plasma was separated by centrifugation.

$CD4^+$ and $CD8^+$ T cell depletion and flow cytometry

Mouse $CD4^+$ and $CD8^+$ T cells were depleted by twice weekly intraperitoneal injections of 200 µg anti-mouse CD4 (GK1.5) (Bio X Cell, West Lebanon, NJ) and 200µg anti-mouse CD8 (2.43) (Bio X Cell, West Lebanon, NJ) diluted in sterile PBS.

The antibodies used to analyze cells isolated from peripheral blood and spleens included antibodies directed against mCD45 (APC-Cy 7, BD Pharmingen, Franklin Lakes, NJ, Cat. 559864), mCD3 (PE, BD Pharmingen, Franklin Lakes, NJ, Cat. 555275), mCD4 (APC, BD Pharmingen, Franklin Lakes, NJ, Cat. 560181), mCD8a (FITC, BD Pharmingen, Franklin Lakes, NJ, Cat. 553030), mCD19 (PE-Cy7, BD Pharmingen, Franklin Lakes, NJ, Cat. 552854) and mCD11b (PerCP, BD Pharmingen, Franklin Lakes, NJ, Cat. 550993). Live cells were distinguished by forward and side scatter profiles. Data was acquired with a BD FACSCanto flow cytometer and analyzed with BD FACS Diva software (v. 6.1.3).

Collection and processing of tissues

Mouse tissues were collected essentially as previously described (42-45). Tissues collected for analysis (depending on mouse gender) included the spleen, bone marrow, lungs, liver, gastrointestinal tract, brain, eyes, FRT, epididymis, testes, prostate, penis, and seminal vesicles. For ZIKV-RNA analysis, tissues were processed into single cell suspensions as previously described (36-39). In brief, cells were isolated by forcing tissues through a 70 µm cell strainer (Falcon, Corning, NY) followed by red blood cell lysis if necessary. The liver, lung, female reproductive tract, and penis were digested in an enzyme digest cocktail prior to filtration. Liver, lung, and brain cells were purified with percoll gradients (GE Healthcare, Little Chalfont, UK). The mouse gastrointestinal tract was flushed with PBS and incubated with a dithiothreitol (Fisher Scientific, Hampton, NC) and EDTA solution to isolate cells from the intraepithelial layer and incubated with elastase (Worthington Biochemical, Lakewood, NJ) and hyaluronidase (Worthington Biochemical, NJ) to isolate the cells from the lamina propria layer (45).

ZIKV-RNA analysis

RNA was extracted from plasma (40 µL) using the QIAmp Viral RNA kit (Qiagen). Tissue RNA was extracted using RNeasy mini columns (Qiagen) according to the manufacture's protocol including an optional treatment with RNase-free DNase. ZIKV-RNA levels in the peripheral blood plasma from infected mice were measured using a one-step quantitative real-time PCR (TaqMan® RNA to-CT 1-step kit, Applied Biosystems, Foster City, CA). The sequences of the forward and reverse primers and the TaqMan® probe for PCR amplification and detection of ZIKV RNA were: 5′-CCGCTGCCCAACACAAG -3′, 5′-CCACTAACGTTCTTTTGCAGACAT -3′, and 5′-FAM-AGCCTACCT/ZEN/TGACAAGCAGTCAGACACACTCAA-Q-3′, respectively (46). ZIKV-RNA was transcribed using a custom synthesized plasmid (Biomatik) to create a standard curve. Sample RNA was quantified by using a standard curve. All samples were run and analyzed on an ABI 7500 Fast Real Time PCR System (Applied Biosystems, Foster City, CA).

Statistical Analysis

If not otherwise specified, sample means are reported along with the corresponding standard error (s.e.m.) which conveys information about the level of imprecision. The estimators and statistical test procedures used in this study are described in the figure legends and in the narrative text in the results section.

To ensure appropriate blinding, the investigators involved in analyzing tissue samples for viral loads were given numbered samples and were thus unable to know treatment group identity (treated, controls). No other blinding procedures were used in the study. No statistical methods were used to pre-determined sample size. No randomization was used to allocate animals/samples to experimental groups.

All statistical computations were performed using GraphPad Prism (version 6.0 for Mac, GraphPad Software, La Jolla, California).

REFERENCES

1. Agrelli A, de Moura RR, Crovella S, Brandao LAC. 2019. ZIKA virus entry mechanisms in human cells. Infect Genet Evol 69:22-9.

2. Junjhon J, Lausumpao M, Supasa S, Noisakram S, Songjaeng A, Saraithong P, Chaichoun K, Utaipat U, Keelapang P, Kanjanahaluethai A, Puttikhunt C, Kasinrerk W, Malasit P, Sittisombut N. 2008. Differential modulation of prM cleavage, extracellular particle distribution, and virus infectivity by conserved residues at nonfurin consensus positions of the dengue virus pr-M junction. J Virol 82:10776-91.

3. Cruz-Oliveira C, Freire JM, Conceicao TM, Higa LM, Castanho MARB, Da Poian AT. 2015. Receptors and routes of dengue virus entry into the host cells. FEMS Microbiol Rev 39:155-70.

4. Bressanelli S, Stuasny K, Allison SL, Stura EA, Duquerroy S, Lescar J, Heinz FX, Rey FA. 2004. Structure of a flavivirus envelope glycoprotein in its low-pH-induced membrane fusion conformation. EMBO J 23(4):728-38.

5. Modis Y, Ogata S, Clements D, Harrison SC. 2004. Structure of the dengue virus envelope protein after membrane fusion. Nature 427(6972): 313-9.

6. Lindenbach BD, Rice CM. 2001. Flaviviridae: The Viruses and Their Replication. Fields Virolofy 4th edn. Knipe DM, Howley PM, editors. pp 991-1041.

7. Murray CL, Jones CT, Rice CM. 2008. Architects of assembly: rls of Flaviviridae non-structural proteins in virion morphogenesis. Nat Rev Microbiol 6(9):699-708.

8. Cortese M, Goellner S, Acosta EG, Neufeldt CJ, Oleksiuk O, Lampe M, Haselmann U, Funaya C, Schieber N, Ronchi P, Schorb M, Pruunsild P, Schwab Y, Chatel-Chaix L, Ruggieri A, Bartenschlager R. 2017. Ultrastructural characterization of zika virus replication factories. Cell Rep 18(9):2113-23.

9. Youn S, Ambrose RL, Mackenzie JM, Diamond MS. 2013. Non-structural protein-1 is required for west nile virus replication complex formation and viral RNA synthesis. Virol J 10:339.

10. Lescar J, Soh S, Lee LT, Vasudevan SG, Kang C, Lim SP. 2018. The dengue virus replication complex: from RNA replication to preotein-protein interactions to evasion of innate immunity. Adv Exp Med Biol 1062:115-29.

11. Leung JY, Pijlman GP, Kondratieva N, Hyde J, Mackenzie JM, Khromykh AA. 2008. Role of nonstructural protein NS2A in flavivirus assembly. J Virol 82:4731-41.

12. Nambala P, Wen-Chi Su. 2018. Role of zika virus prM protein in viral pathogenicity and use in vaccine development. Front Microbiol 9:1797.

13. Yu IM, Zhang W, Holdaway HA, Li L, Kostyuchenko VA, Chipman PR, Kuhn RJ, Rossmann MG, Chen J. 2014. Structure of the immature dengue virus at low pH primes proteolytic maturation. Science 80(319):1834-7.

14. Rey A, Stiasny K, Heinz FX. 2017. Flavivirus structural heterogeneity: implications for cell entry. Curr Opin Virol 24:132-9.

15. Kim SY, Li B, Linhardt RJ. 2017. Pathogenesis and inhibition of flaviviruses from a carbohydrate perspective. Pharmacueticals 10:1-24.

16. Mercer J, Helenius A. 2010. Apoptotic mimicry: phosphatidylserine-mediated micropinocytosis of vaccinia virus. Ann NY Acad Sci 1209:49-55.

17. Kaksonen M, Roux A. 2018. Mechanisms of clathrin-mediated endocytosis. Nat Rev Mol Cell Biol 19(5):313-26.

18. Yoon KJ, Song G, Qian X, Pan J, Xu D, Rho HS, Kim NS, Habela C, Zheng L, Jacob F, Zhang F, Lee EM, Huang WK, Ringeling FR, Vissers C, Li C, Yuan L, Kang K, Kim S, Yeo J, Cheng Y, Liu S, Wen Z, Qin CF, Wu Q, Christian KM, Tang H, Jin P, Xu Z, Qian J, Zhu H, Song H, Ming GL. 2017. Zika-virus-encoded NS2A disrupts mammalian cortical neurogenesis by degrading adherens junction proteins. Cell Stem Cell 21:349-58.

19. Cao B, Diamond MS, Mysorekar IU. 2017. Maternal-Fetal Transmission of Zika Virus: Routes and Signals for Infection. J Interferon Cytokine Res 37(7):287-94.

20. Coelho AVC, Crovella S. 2017. Microcephaly Prevalence in Infants Born to Zika Virus-Infected Women: A Systematic Review and Meta-Analysis. Int J Mol Sci 18(8):1714.

21. De Araújo TVB, Rodrigues LC, de Alencar Ximenes RA, de Barros Miranda-Filho D, Montarroyos UR, de Melo APL, Valongueiro S, de Albuquerque FPM, Souza WV, Braga C, et al. 2016. Association between zika virus infection and microcephaly in Brazil, January to May, 2016: preliminary report of a case-control study. Lancet Infect Dis 16:1356–63.

22. Dirlikov E, Major CG, Medina NA, Lugo-Robles R, Matos D, Muñoz-Jordan JL, Colon-Sanchez C, Garcia M, Olivero-Segarra M, Malave G, Rodríguez-Vega GM, Thomas DL, Waterman SH, Sejvar JJ, Luciano CA, Sharp TM, Rivera-García B. 2018. Clinical Features of Guillain-Barré Syndrome With vs Without Zika Virus Infection, Puerto Rico, 2016. JAMA Neurol 75(9):1089–97.

23. Rivera-Concepcion JR, Betancourt JP, Cerra J, Reyes E. 2018. the zika virus: an association to guillain-Barré syndrome in the united states – a case report. P R Health Sci J. 37(Special Issue): S93-5.

24. Hermanns K, Gohner C, Kopp A, Schmidt A, Merz WM, Markert UR, Junglen S, Drosten C. 2018. Zika virus infection in human placental tissue explants is enhanced in the presence of dengue virus antibodies in-vitro. Emerg Microbes Infect 7(1):198.

25. Dejnirattisai W, Supasa P, Wongwiwat W, Rouvinski A, Barba-Spaeth G, Duangchinda T, Sakuntabhai A, Cao-Lormeau V, Malasit P, Rey FA, Mongkolspaya J, Screaton G. 2016. Dengue virus sero-cross reactivity drives antibody-dependent enhancement of infection with zika virus. Nat Immunol 17(9):1102-8.

26. Lazear HM, Govero J, Smith AM, Platt DJ, Fernandez E, Miner JJ, Diamond MS. 2016. A Mouse Model of Zika Virus Pathogenesis. Cell Host Microbe 19:720-30.

27. Rossi SL, Tesh RB, Azar SR, Muruato AE, Hanley KA, Auguste AJ, Langsjoen RM, Paessler S, Vasilakis N, Weaver SC. 2016. Characterization of a Novel Murine Model to Study Zika Virus. Am J Trop Med Hyg 94:1362-9.

28. Kalkeri R, Krishna KM. 2017. Zika virus reservoirs: implications for transmission, future outbreaks, drug and vaccine development [version 1; referees: 2 approved]. F1000Research 6:1850.

29. Mlera L, Melik W, Bloom ME. 2014. The role of viral persistence in flavivirus biology. Pathog Dis 71(2):137-63.

30. Ravi V, Desai AS, Shenoy PK, Satishchandra P, Chandramuki A, Gourie-Devi M. 1993. Persistence of Japanese encephalitis virus in the human nervous system. J Med Virol 40(4):326-9.

31. Atkinson B, Thorburn F, Petridou C, Bailey D, Hewson R, Simpson AJ, Brooks TJ, Aarons EJ. 2017. Presence and persistence of zika virus RNA in semen, United Kingdom, 2016. Emerg Inf Dis 23(4):611-5.

32. Ma W, Li S, Jia L, Zhang F, Zhang Y, Zhang J, Wong G, Zhang S, Lu X, Liu M, Yan J, Li W, Qin C, Han D, Qin C, Wang N, Li X, Gao GF. 2017. Zika virus causes testis damage and leads to male infertility in mice. Cell 167(6):1511-24.

33. Bhatnagar J, Rabenack DB, Martines RB, Reagan-Steiner S, Ermias Y, Estetter LB, Suzuki T, Ritter J, Keating MK, Hale G, Gary J, Muehlenbachs A, Lambert A, Lanciotti R, Oduyebo T, Meaney-Delman D, Bolaños F, Saad EA, Shieh WJ, Zaki SR. 2017. Zika virus RNA replication and persistence in brain and placental tissue. Emerg Infect Dis 23(3):405-11.

34. Kodati S, Palmore TN, Spellman FA, Cunningjam D, Weistrop B, Sen HN. 2017. Bilateral posterior uveitis associated with zika virus infection. Lancet 389(10064):125-6.

35. Nicastri E, Castilletti C, Liuzzi G, Iannetta M, Capobianchi MR, Ippolito G. 2016. Persistent detection of zika virus RNA in semen for six months after symptom onset in a traveler returning from Haiti to Italy, February 2016. Euro Surveill 21(32):30314.

36. Rossini G, Gaibani P, Vocale C, Cagarelli R, Landini MP. 2017. Comparison of zika virus (ZIKV) RNA detection in plasma, whole blood and urine – Case series of travel-associated ZIKV infection imported to Italy, 2016. J Infect 75(3):242-5.

37. Sun JW, Zhong H, Guan D, Zhang H, Tan Q, Ke C. 2016. Presence of zika virus in conjunctivital fluid. Opthamol 134(11):1330-2.

38. Grant A, Ponia SS, Tripathi S, Balasubramaniam V, Miorin L, Sourisseau M, Schwarz MC, Sáchez-Seco MP, Evans MJ, Best SM, García-Sastre A. 2016. Zika virus targets human STAT2 to inhibit type I interferon signaling. Cell Host Microbe 19(6):882-90.

39. Kumar A, Hou S, Airo AM, Limonta D, Mancinelli V, Branton W, Power C, Hobman TC. 2016. Zika virus inhibits type-I interferon production and downstream signaling. EMBO Rep 17(12):1766-75.

40. Miner JJ, Sene A, Richner JM, Smith AM, Santeford A, Ban N, Weger-Lucarelli J, Manzella F, Rückert C, Govero J, Noguchi KK, Ebel GD, Diamond MS, Apte RS. 2016. Zika virus infection in mice causes panuveitis with shedding of virus in tears. Cell Rep 16(12):3208-18

41. Zhao Z, Yang M, Azar SR, Soong L, Weaver SC, Sun J, Chen Y, Rossi SL, Cai J. 2017. Viral retinopathy in experimental models of Zika infection. Invest Ophthalmol Vis Sci 58(10):4355-65.

42. Denton PW, Estes JD, Sun Z, Othieno FA, Wei BL, Wege AK, Powell DA, Payne D, Haase AT, Garcia JV. 2008. Antiretroviral pre-exposure prophylaxis prevents vaginal transmission of HIV-1 in humanized BLT mice. PLoS Med 5:e16.

43. Olesen R, Wahl A, Denton PW, Garcia JV. 2011. Immune reconstitution of the female reproductive tract of humanized BLT mice and their susceptibility to human immunodeficiency virus infection. J Reprod Immunol 88:195-203.

44. Denton PW, Nochi T, Lim A, Krisko JF, Martinez-Torres F, Choudhary SK, Wahl A, Olesen R, Zou W, Di Santo JP, Margolis DM, Garcia JV. 2012. IL-2 receptor gamma-chain molecule is critical for intestinal T-cell reconstitution in humanized mice. Mucosal Immunol 5:555-66.

45. Shanmugasundaram U, Kovarova M, Ho PT, Schramm N, Wahl A, Parniak MA, Garcia JV. 2016. Efficient Inhibition of HIV Replication in the Gastrointestinal and Female Reproductive Tracts of Humanized BLT Mice by EFdA. PLoS One 11:e0159517.

46. Lanciotti RS, Kosoy OL, Laven JJ, Velez JO, Lambert AJ, Johnson AJ, Stanfield SM, Duffy MR. 2008. Genetic and serologic properties of Zika virus associated with an epidemic, Yap State, Micronesia, 2007. Emerg Infect Dis 14:1232-9.

CHAPTER 2: PHARMACOLOGICAL AND IMMUNOLOGICAL CONTROL OF ZIKA VIRUS REPLICATION IN MICE DEFICIENT IN ADAPTIVE IMMUNE RESPONSES – REFORMATTED MANUSCRIPT DRAFT

Introduction

Zika virus (ZIKV) is a mosquito-transmitted small-enveloped positive-stranded RNA virus from the Flavivirus genus in the Flaviviridae family that has emerged as a human pathogen with epidemic potential (1). Until 2007, only sporadic outbreaks of ZIKV infection involving no more than a few persons had occurred, usually resulting in a mild infection causing a self-limiting fever, headache, myalgia, rash, and conjunctivitis (1). However, recent outbreaks in Micronesia in 2007 (2, 3), French Polynesia in 2013-2014 (4, 5), and the Americas in 2015-2016 (6-8) revealed that ZIKV infections, can be prolonged and cause more severe clinical consequences including Guillain-Barré syndrome in adults and microcephaly and congenital malformations in fetuses and newborn infants (9). Unlike other flaviviruses, ZIKV has the potential for significant horizontal transmission due to shedding in bodily fluids long after symptom onset (10-14). Given the severe clinical consequences and potential for ZIKV spread, vaccine development is important. However, development of clinical strategies needed for treatment during epidemics when prevention of infection is no longer an option is paramount. Animal models capable of recapitulating chronic and persistent ZIKV infection will be critical to understand pathogenic mechanisms of ZIKV infection and to evaluate novel treatment strategies.

Inoculation of immune competent, wild type mice (C57BL/6, BALB/c or CD-1 mice) with ZIKV strains from Africa, French Polynesia, Brazil, or Puerto Rico does not result in disease and little to no infectious virus or viral RNA is detected in tissues (15-17). The resistance of immune competent mouse strains to ZIKV infection is due to the inability of ZIKV to antagonize the mouse type I interferon (IFN) response (18, 19). As a result, most mouse models of ZIKV infection have genetic deficiencies in the IFN signaling pathway.

Mice lacking the interferon alpha/beta receptor 1 (Ifnar1), like A129 mice, Ifnar1-/- C57BL/6 mice, mice deficient in Irf3, Irf5, and Irf7 or STAT2 deficient mice support ZIKV infection (16, 17, 20). When inoculated with African (MR 766 or Dakar 1984), Asian (H/PF/2013), or American (Brazil Paraiba_2015) ZIKV strains (16, 17, 20-22) these mice develop disease symptoms including hind limb weakness, paralysis, and death. Mice deficient in both type I and type II IFN receptors (AG129) show greater susceptibility and more severe disease following ZIKV infection (17, 23-26). Although severity of disease and lethality is age-dependent in these models, most mice die within 1 month of ZIKV infection (16, 17, 27).

In an alternative approach, type I IFN signaling in wild type (WT) C57BL/6 mice is suppressed with anti-IFNAR1 monoclonal antibody (mAb) prior to and after virus inoculation. Suppression, rather than complete abrogation, of the type I IFN response in this manner may more accurately reflect ZIKV infection and transmission in humans. This also allows the analysis of other components of the immune response during ZIKV transmission (26). Anti-IFNAR1 mAb treated mice inoculated with ZIKV Dakar strains exhibited high levels of ZIKV-RNA in serum, weight loss and mortality compared to control mice (28). However, a less severe phenotype without weight loss or death after infection was observed when anti-IFNAR1 mAb treated mice were inoculated with an Asian ZIKV strain (H/PF/2013) (16). Similarly, WT mice treated with the anti-inflammatory steroid dexamethasone prior to and after intraperitoneal inoculation with a Puerto Rican ZIKV strain (PRVABC59) experienced weight loss, viremia, and a disseminated infection. Dexamethasone withdrawal after infection led to rapid deterioration of the mice that was associated with inflammation and injury in the brain, kidneys, and testes (29). An additional mouse model of ZIKV infection is the highly immune deficient anti-IFNAR1 mAb treated Rag1−/− (AIR) mouse. Rag1−/− mice lack adaptive immune responses but are not susceptible to ZIKV infection. The AIR variant requires anti-IFNAR1 antibody administration every 2-4 days and is permissive to ZIKV infection, with virus in the testes, spleen, and brain (30). Disease progression is slower in AIR mice compared to other mouse models permissive to ZIKV infection, severe weight loss is not observed until 14-17 dpi (22, 30). While the AIR model might be somewhat more relevant to the study of acute infection than the other models described above, none of those mouse strains seem to model chronic and persistent infection.

Here, we describe three different immune deficient mouse strains (NOD/SCID, NSG and NOG) that support high and sustained levels of chronic virus replication with delayed onset of disease. These strains are immune deficient by virtue of a lack of B cells, T cells, and NK cells but have a full complement of interferon and interferon-receptor genes. Inoculation of these mice with ZIKV results in high viremia, systemic dissemination to all tissues tested, delayed signs of illness and a half-life of up to 56 days post infection. The fact that these mice do not need anti-interferon treatment before or during ZIKV infection 1) greatly simplifies their use, 2) increases reproducibility and 3) lowers costs. We used these three immune deficient mouse strains for the evaluation of novel interventions for the treatment of ZIKV infection through the administration of a pharmacological intervention and a neutralizing antibody, both of which significantly reduced peripheral viral-RNA during and after administration. The neutralizing antibody was also demonstrated to prevent shedding in the saliva and reduce viral-RNA found in critical tissues such as the male genital tract and female reproductive tract.

Results

Immune deficient mice lacking T cells, B cells, and NK cells maintain high levels of ZIKV-RNA in the periphery. W intravenously exposed immune deficient NSG mice that lack T cells, B cells, and NK cells using decreasing inoculum doses; 2.5 x 10^4 FFU, 5.0 x 10^3 FFU, 1.0 x 10^3 FFU, and 0.3 x 10^3 FFU ZIKV H/PF/2013. As NSG mice maintained a robust peripheral infection even at low inoculum doses. At 0.3 x 10^3 FFU, 2/3 mice had detectable ZIKV-RNA. One mouse had only a low quantity of detectable virus two days post exposure which did not become detectable again. ZIKV-RNA was undetectable in the second mouse at that inoculum dose until 42 days post exposure, at which point it established a robust infection which was maintained through the course of the experiment (Figure 2.1). At 1.0 x 10^3 FFU, 0/3 mice had detectable virus through 120 days post exposure. At 5.0 x 10^3 FFU, 2/3 mice had detectable virus by 35 days post exposure that replicated efficiently reaching as high as 10^8 ZIKV-RNA copies/mL plasma. The 2.5 x 10^4 FFU group was the only one to have a 100% rate of infection by two days post exposure. This was maintained for the course of the experiment and the mice achieved a similar peak viral load to the infected mice in the 5.0 x 10^3 FFU group. Most striking, however, was the protracted survival of the NSG mice despite highly productive infections compared to other commonly used mouse models of ZIKV infection.

The minimum inoculum dose that had 100% rate of infection in our samples sizes of n=3 was 2.5 x 10^4 FFU ZIKV H/PF/2013. To ensure consistency of infection and pathology, we used a minimum of 10X that amount, 2.5 x 10^5 FFU ZIKV H/PF/2013 in future experiments.

Sustained high-level systemic replication of ZIKV in immune deficient mice. To further evaluate the importance of the adaptive immune system in ZIKV infection, we intravenously infected one mouse strain that is deficient in T cells and B cells (NOD/SCID) and two mouse strains that are deficient in T cells, B cells, and NK cells (NOG and NSG) with 0.5-1.0 x 10^6 FFU of ZIKV H/PF/2013 (n = 4, 4, and 3, mice respectively, all females). Approximately 1000-fold higher levels of ZIKV-RNA in plasma compared to BALB/c mice were detected as early as two days post exposure in all animals regardless of strain. Also, in sharp contrast to BALB/c mice, longitudinal analysis of infection demonstrated high and sustained levels of ZIKV-RNA in all three strains of mice (Figure 2.2, panels A-C). Infection of NSG males also led to sustained high levels of ZIKV-RNA in plasma (Figure 2.2D). Under our experimental

conditions, we observed similar mean levels of plasma ZIKV-RNA and survival in male and female mice. The logrank test for a sex effect was not statistically significant ($p > 0.05$) (Supplementary Figure 2.1A). The replication competence of the ZIKV found in plasma from infected NSG mice was verified both *in vitro* and *in vivo*. For *in vitro* analysis, serum from infected NSG mice (3uL) was added to Vero cells, and ZIKV-RNA was quantified in culture medium 24h, 48h, and 96h later. Levels of ZIKV-RNA in culture medium increased exponentially over time (Supplementary Figure 2.2A), indicating efficient replication of ZIKV from infected mice in VERO cell culture. For *in vivo* testing, serum was collected from 3 ZIKV infected NSG mice on days 21 and 28 post-inoculation. Serum was pooled, and 60 µl used for inoculation of two naïve NSG mice (Supplementary Figure 2.2B). Levels of ZIKV-RNA in plasma of serum-exposed mice increased rapidly and were maintained throughout the experiment (56 and 65 days, respectively) (Supplementary Figure 2.2C) providing further evidence that ZIKV in infected NSG mice was replication competent.

In humans, an important characteristic of ZIKV infection is the presence of virus in bodily secretions (saliva, vaginal secretions, breast milk, urine, and semen)(31-34). We evaluated the presence of virus in the saliva of infected mice. High levels of ZIKV-RNA were found in saliva (Figure 2E). Similarly, ZIKV-RNA was consistently present in the urine and cervicovaginal secretions of infected mice (Supplementary Table 2.1).

In contrast to BALB/c mice that survived for almost a year post infection, over time, immune deficient mice succumbed to infection (Figure 2.2F). All NOG mice died within the first 47 days post-infection (half-life 26 days post-exposure). The half-life of NOD/SCID and NSG mice was four weeks longer (54 and 56 days, respectively). ZIKV-infected male and female mice were similar in survival (Supplementary Figure 2.1B). The logrank test for a sex difference was not statistically significant ($p = 0.83$).

To establish the ability of different strains of ZIKV to replicate in immune deficient mice, we inoculated NSG mice with three additional strains of ZIKV from recent outbreaks in the western hemisphere including one strain from Puerto Rico (PRVABC59) and two strains representing distinct ZIKV clades from Brazil (SPH2015 and BEH 819015). As early as two days post-inoculation, all three strains showed robust levels of virus replication in plasma that were sustained throughout the experiment (Figure 2.2G-I).

Together, these results demonstrate the susceptibility of immune deficient mouse strains to ZIKV infection without the need for preconditioning or any other type of intervention like anti-interferon treatment, characterized by robust and sustained replication with a protracted half-life.

Systemic replication of ZIKV in tissues from immune deficient mice. To establish the systemic replication of ZIKV during acute and chronic infection, cell-associated ZIKV-RNA in infected NSG mice (n = 11 acute, n = 12 chronic) was evaluated using quantitative real-time PCR analysis from bone marrow, spleen, liver, lung, brain, gut epithelium, gut lamina propria, and the eye (Figure 2.3A). During acute infection (two days post exposure), high levels of ZIKV-RNA were detected in the plasma of all animals. However, levels of cell-associated ZIKV-RNA were variable in the different tissues analyzed. For example, whereas ZIKV-RNA was readily detected in the spleen, liver, lung, gut lamina propria and eyes from the majority of mice, ZIKV-RNA was only detected in the bone marrow and brain of approximately half of the animals. In contrast, during chronic ZIKV infection (27-73 days post exposure) statistically significantly higher levels of virus were found in all tissues analyzed. Of these tissues, the brain ($2.50 \times 10^8 \pm 1.05 \times 10^8$ s.e.m. ZIKV-RNA copies per 10^5 cells) and the eye ($1.14 \times 10^8 \pm 0.84 \times 10^8$ s.e.m. ZIKV-RNA copies per eye) had the highest levels of ZIKV-RNA. These results demonstrate that ZIKV rapidly establishes a systemic infection in immune deficient mice that is maintained at very high levels in all tissues analyzed.

ZIKV replication in the male and female reproductive tracts. Given the importance of sexual transmission of ZIKV, we also determined the presence of ZIKV in the male genital tract (testes, epididymis, prostate, penis, and seminal vesicles) and FRT of immune deficient mice (female: acute n = 4, chronic n = 5; male: acute n = 5 chronic n = 5). Remarkably, two days post-infection, all male animals had readily detectable levels of ZIKV-RNA in the testes and all female animals in their reproductive tract (Figure 2.3B). In some male animals, ZIKV-RNA was also noted in the epididymis, prostate and seminal vesicles (Figure 2.3B). We did not detect ZIKV-RNA in the penis during acute infection. During chronic infection, ZIKV-RNA was consistently detected at statistically significantly higher levels in all tissues of the male reproductive tract, including the penis (testes p=0.0079, epididymis p=0.0079, penis p=0.0286, prostate p=0.0159, seminal vesicles p=0.0159, Mann-Whitney test). The highest viral burden was observed in the epididymis and the testes followed by the prostate, seminal vesicles and penis. Similarly,

the levels of ZIKV-RNA in the FRT were statistically significantly higher during chronic infection (p=0.0159, Mann Whitney test). These results demonstrate that ZIKV is consistently present in the male and female reproductive tracts during acute ZIKV-infection and that ZIKV replication in sustained at high levels in these compartments during chronic infection.

7-Deaza-7-fluoro-2'-C-methyl-adenoside (DFMA) reduces viral burden and improves survival after ZIKV infection. Currently there are no approved treatments for ZIKV infection. Recently, the nucleoside DFMA (Supplementary Figure 2.3) was reported to have anti-ZIKV activity (35). The ability of ZIKV to replicate efficiently and for prolong periods of time in immune deficient mice allows for the *in vivo* evaluation of novel viral inhibitors like DFMA. Beginning two days prior to infection with ZIKV H/PF/2013 (2.5×10^5 FFU) (Figure 2.4), NSG mice were administered DFMA (n = 6, 10 mg/kg per day, i.p.) or vehicle (n = 4) daily for 21 days (until 19 days post-exposure with ZIKV). Plasma ZIKV-RNA levels were monitored over time. At two days post exposure, the levels of viremia in DFMA treated and control groups were similar. However, as early as four days post-infection, ZIKV-RNA levels in the plasma of DFMA treated mice ($9.41 \times 10^5 \pm 1.40 \times 10^5$ s.e.m. ZIKV-RNA) were statistically significantly lower compared to control animals ($2.00 \times 10^6 \pm 2.90 \times 10^5$ s.e.m. ZIKV-RNA) (Figure 2.4, panels A and B). Statistically significantly lower levels of ZIKV-RNA were consistently observed in the plasma of DFMA treated mice compared to controls during the duration of treatment. Surprisingly, although DFMA treatment was discontinued after 21 days, statistically significantly lower levels of viremia were observed in DFMA treated mice up to three weeks post-treatment discontinuation (Figure 2.4, A and B). All 4 animals in the control group succumbed to infection by 57 days post-exposure (Figure 2.4, C and D). Only 2/6 DFMA treated animals succumbed to infection ($p < 0.05$) (Figure 2.4, C and D). These results demonstrate that DFMA treatment reduces viremia and reduces mortality of ZIKV infected mice.

Pretreatment with C10, a neutralizing anti-ZIKV antibody, markedly reduces virus replication, shedding and overall plasma viral burden. C10 is a dengue virus serotype cross-neutralizing monoclonal antibody isolated from a dengue patient. It was previously shown to neutralize ZIKV in cell culture and reduce ZIKV-induced morbidity and mortality in a type I/II interferon receptor-knockout murine model (36). To investigate the effect of C10 pre-exposure prophylaxis on the establishment of ZIKV infection, replication and pathogenesis, mice received one systemic administration

of C10 intraperitoneally (62.5 µg, n = 10) or control antibody (62.5 µg IgG, n = 9). Mice were exposed to ZIKV H/PF/2013 intravenously (2.5 x 10^5 FFU) 18 h after treatment and ZIKV infection was monitored in peripheral blood for six weeks.

All mice treated with control antibody became infected. High levels of ZIKV-RNA were detected in the plasma of all control animals by two days post-exposure (1.15 x 10^6 ± 5.23 x 10^4 s.e.m. ZIKV-RNA copies/mL) and viremia was maintained for six weeks (last time point analyzed) (Figure 2.5, panels A and B). In stark contrast, there was no evidence of peripheral blood infection in 7/10 C10-treated mice. Low levels of ZIKV-RNA were only transiently observed immediately after infection in three animals. Specifically, ZIKV-RNA was not detected in the plasma from 7/10 C10-treated mice two days post-exposure and low levels (1,722 ± 307 copies/mL) were detected in three ZIKV-positive mice (Figure 2.5B). Seven days post exposure, plasma ZIKV-RNA levels were undetectable in all treated mice (Figure 2.5B). ZIKV-RNA was undetectable through 35 days post exposure in most of the animals, with only three transient instances of detectable viral-RNA in 2/10 animals. By six weeks post exposure, only 4/10 mice had low but detectable levels of ZIKV-RNA in plasma (5,125 ± 2,023 copies per mL).

C10 pre-exposure prophylaxis also efficiently inhibited ZIKV-RNA shedding. ZIKV-RNA levels were undetectable in saliva collected from all (10/10) C10-treated mice 30 days post ZIKV exposure. In contrast, high levels of ZIKV-RNA were present in the saliva of control mice (1.64 x 10^5 ± 5.62 x 10^4 s.e.m copies/mL) (Figure 2.5C). During the course of the experiment (42 days), no C10-treated mice succumbed to infection or showed any signs of illness. However, 2/9 control mice succumbed to infection by 26 days post-exposure (Figure 2.5D). These data demonstrate that a single dose of C10 administered prior to ZIKV exposure effectively inhibits ZIKV replication *in vivo* over an extended period of time and markedly reduces (>2,000-fold) ZIKV-RNA levels in plasma and saliva ($p < 0.0001$).

A single dose of C10 greatly reduces ZIKV replication in tissues. Successful ZIKV therapy depends on the ability of the treatment to penetrate to affected tissues. To investigate the effect of C10 on the levels of ZIKV-RNA in tissues, we harvested C10-treated and control mice six weeks post ZIKV exposure and analyzed cell-associated virus RNA levels in the bone marrow, spleen, liver, lung, gut (intraepithelial and lamina propria layers), brain and eyes (Figure 2.6A). In control mice, ZIKV-RNA was readily found in all tissues from all animals analyzed. The highest levels of viral RNA were observed in

the gut lamina propria, brain, and eyes. In sharp contrast, almost all tissues analyzed from the C10-treated mice had low levels of viral RNA or levels that were below the LOD. In most tissues of C10-treated mice, cell-associated ZIKV-RNA levels were 2-5 logs lower compared to control animals (Figure 2.6A). These results show that C10 effectively reduces the systemic levels of cell-associated ZIKV-RNA (Figure 2.6A).

C10 efficiently suppresses ZIKV replication in the male and female reproductive tracts. Because of their relevance to sexual ZIKV transmission, we evaluated the effect of C10 pre-treatment on the levels of virus in the different organs of the male genital tract (testes, epididymis, prostate, penis, and seminal vesicles) and FRT. ZIKV-RNA was readily detected in the epididymis, penis, prostate, seminal vesicles and testes of all control male animals (Figure 2.6B). In contrast, ZIKV-RNA levels were statistically significantly lower in all of the male genital tract tissues from C10-treated animals, and in most samples below our assays ability to detect (Figure 2.6B). ZIKV-RNA was also consistently detected in FRT of all female animals administered the control antibody. However, statistically significantly lower levels of ZIKV-RNA were observed in the FRT from C10-treated animals (Figure 2.6B). Collectively, these results demonstrate that a single administration of C10 efficiently inhibits ZIKV replication in the male and female reproductive tracts for at least 6 weeks.

Discussion

During human ZIKV infection, the ZIKV NS5 protein inhibits STAT2, thereby suppressing the type I IFN response to ZIKV allowing for viral replication and dissemination. As a result, replication-competent infection has been verified in the female reproductive tract, the placenta and fetal tissue, in neural progenitor and adult neural cells, and in immune privileged tissues such as the testes and the eyes. ZIKV shedding has also been observed in humans in breast milk, saliva, urine, semen, and cervical mucus, which may contribute to vectorless transmission (37). In newborns, ZIKV infection results in severe eye disease characterized by optic neuritis, chorioretinal atrophy and blindness (9, 38). In adults, ZIKV infection can result in conjunctivitis and uveitis (39, 40).

Growing evidence suggests that the immune response to ZIKV in mice is more complex than just type I interferon and that other components of the immune system may be able to control ZIKV infection. For example, WT C57BL/6 mice treated with anti-IFNAR antibodies have a suppressed, but not completely deficient IFN response, and develop viremia when inoculated with Asian ZIKV strains. However, they do not lose weight or develop neurologic disease (16). Mice deficient in MAVS, an adaptor of cytosolic RIG-I–like receptors signaling, develop an acute infection after ZIKV exposure, but only experience significant weight loss when their $CD4^+$ and $CD8^+$ T cells are depleted (22). ZIKV-infected AIR mice, Rag1-/- mice deficient in functional T and B cells and IFN responses suppressed with anti-IFNAR Abs, have high levels of viral RNA in the spleen, lymph nodes, and brain and exhibit significant weight loss. Thus, both adaptive and innate immune responses appear to be required to control ZIKV replication, its spread and the severity of disease symptoms.

As deficiency in the type I interferon pathway in mice results in severe ZIKV disease and death, mouse models with a deficient adaptive immune response and impaired innate immune response could prove valuable for the study of ZIKV infection with a delayed onset of disease. NSG mice have a *scid* mutation on the NOD/ShiLtJ genetic background and a complete null allele of the IL2 receptor common gamma chain ($IL2rg^{null}$). This renders NSG mice B and T cell deficient, prevents cytokine signaling through multiple receptors, leads to a deficiency in NK cells, and reduces innate immune responses. As reported here, these immune deficient mice are fully permissive for ZIKV infection. Immune deficient mice intravenously inoculated with ZIKV H/PF/2013 had robust plasma viremia detected as early as two

days post-infection that was sustained for up to 91 days (last time point analyzed). ZIKV-RNA was detected in multiple tissues as early as 2 days post-infection, suggesting rapid systemic dissemination. Although the majority of ZIKV-infected NSG mice (75%) eventually succumbed to infection, the half-life of ZIKV-infected NSG mice was 56 days, much longer than other murine models, where the majority of the animals died within 30 days post ZIKV infection (16, 17, 27). Immune deficient NOG mice are phenotypically similar to NSG mice but they express a truncated form of the protein instead of a deletion of the common gamma chain receptor. NOG mice intravenously inoculated with ZIKV H/PF/2013 developed very similar viremia compared to NSG mice, except that all of the animals succumbed to infection by 26 days post-infection. NOD/SCID mice are the parental strain of both NSG and NOG mice and have an intact common gamma chain. When infected with ZIKV, NOD/SCID mice also developed sustained plasma viremia but had a lower initial plasma viral load compared to NSG mice. However, during chronic infection, their plasma viral load, half-life and survival rate was similar to NSG mice. These results suggest a minimal role for the common gamma chain in the progression of ZIKV infection in NSG or NOG mice.

ZIKV infection of immune deficient mice lacking T cells, B cells and NK cells is therefore characterized by: 1) a rapid increase in plasma viremia and subsequent maintenance of a high viral load that allows for the evaluation of therapeutic strategies targeting ZIKV infection during acute and chronic stage of infection; 2) early compartmentalization resulting in very high ZIKV loads in the brain, eye, testes, epididymis, and FRT during chronic stage of infection which is useful for the evaluation of tissue penetration and efficacy of ZIKV therapeutics; 3) ZIKV shedding in saliva, cervicovaginal secretions, and urine, which allows assessment of the role of therapeutics in prevention of sexual and non-sexual ZIKV transmission as well as persistence; and 4) Immune deficient mice do not need anti-interferon treatment before or during ZIKV infection, greatly simplifying the use of this model and lowering its cost.

To further illustrate the utility of immune deficient mice as a model for ZIKV infection, we used a pharmacological approach and an immunological approach to control ZIKV infection. Consistent with the results obtained in IFN knockout mice (AG129), treatment with DFMA demonstrated significant reductions in plasma viral load that extended beyond the period of treatment and resulted in improved survival of infected animals (35). Mice treated with a single injection of C10, a dengue virus envelope dimer epitope

monoclonal antibody (36, 42), prior to ZIKV H/PF/2013 infection had dramatically reduced levels of plasma viremia immediately after exposure. ZIKV-RNA levels in plasma were below or near the LOD for five weeks after infection. Importantly, C10 treatment also prevented ZIKV-RNA shedding in saliva and was very effective in reducing ZIKV-RNA levels in immune privileged tissues including the brain, eye and genital tract. Immune privileged organs are critical to the study of ZIKV drug effectiveness because they have been noted for having some of the highest levels of ZIKV during infection. These results show that C10 treatment could be used as an approach to control life-threatening ZIKV infection (43). It also points to the possibility of repurposing existing treatment for ZIKV (44, 45). This is supported by recent studies showing that sofosbuvir, an FDA-approved nucleotide analog inhibitor of the hepatitis C RNA-dependent RNA polymerase has protective effect against ZIKV in vitro and *in vivo* (46-49).

In conclusion, immune deficient mice provide a robust platform for the long-term evaluation of ZIKV replication and the *in vivo* evaluation of pharmacological and therapeutic approaches to control virus replication and spread within the infected individual and to prevent vertical and horizontal transmission. In addition, the fact that immune deficient mice can be reconstituted with an intact functional immune system or some of its components (T cells, B cells, etc.) provides an opportunity to elucidate how infection is controlled in immune competent subjects.

Author contributions: Conceptualization, N.J.S, A.S.C., R.F.S., A.W., R.S.B., M.K., and J.V.G.; Investigation, N.J.S, A.S.C, W.O.T., R.A.S., P.T.H, and J.B.H., Writing – Original Draft, N.J.S., M.K., and J.V.G.; Writing – Review & Editing, A.S.C., R.F.S., A.W., R.S.B. and J.V.G; Funding Acquisition, R.S.B.and R.F.S.; Resources, A.S.C., F.A., L.B, R.S.B., and R.F.S., Supervision, R.S.B., R.F.S., and J.V.G.

Declaration of Interests: The authors declare no competing interests.

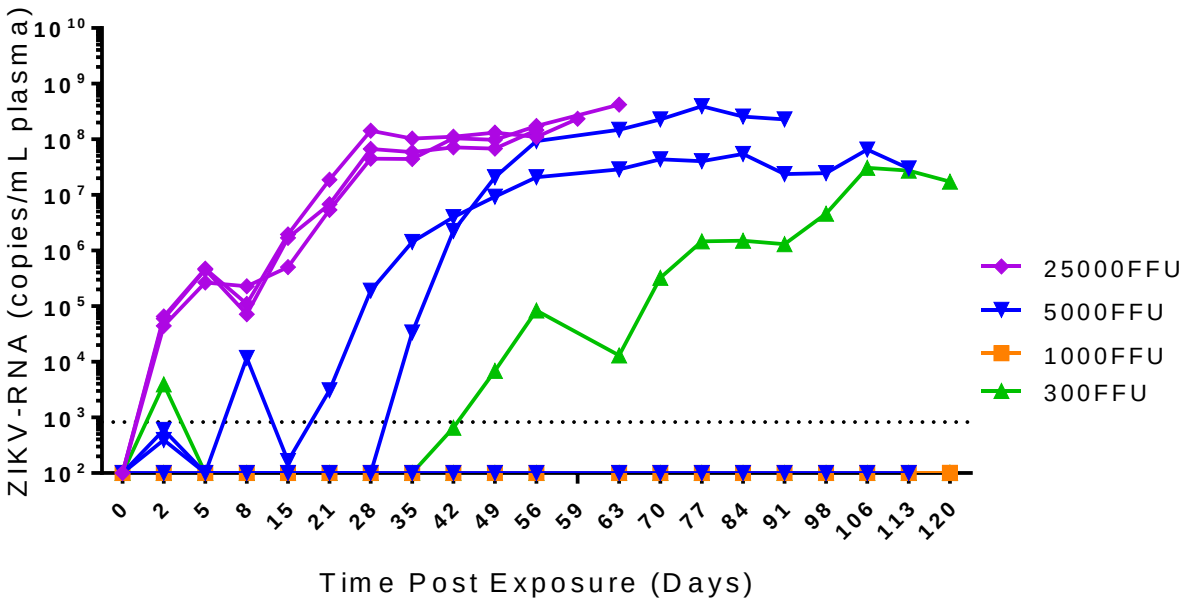

Figure 2.1. Immune deficient NSG mice are permissive to ZIKV infection. Analysis of ZIKV-RNA in plasma NSG mice exposed to ZIKV H/PF/2013 (n=3 mice in each group). Mice were intravenously exposed to ZIKV H/PF/2013 using 2.5 x 10^4 FFU (Purple diamonds), 5.0 x 10^3 FFU (Blue inverted triangles), 1.0 x 10^3 FFU (Orange squares), and 0.3 x 10^3 FFU (Green triangles). The dashed line represents the lowest quantified standard in the PCR assay and is equivalent to 833 copies per mL plasma.

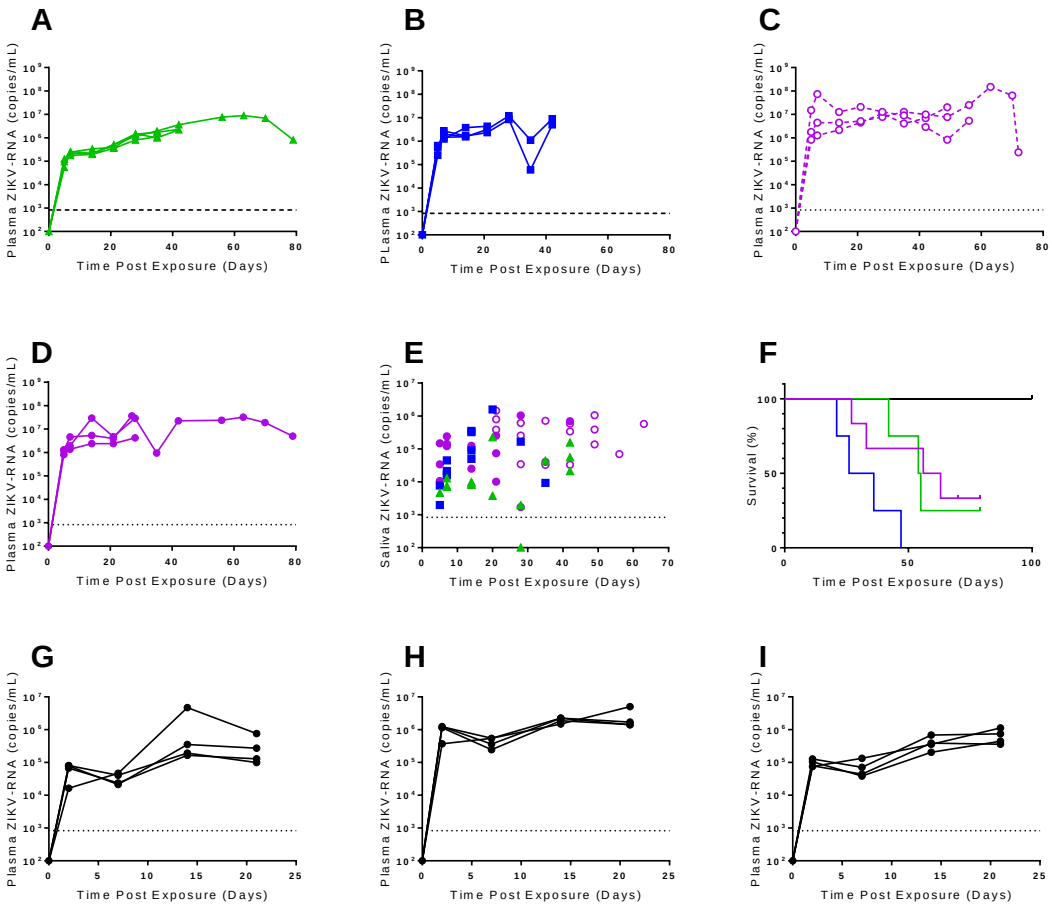

Figure 2.2. Sustained plasma viremia and viral shedding in the saliva of ZIKV-infected immune deficient mice. ZIKV-RNA levels in the plasma of (A) NOD/SCID (n = 4 females), (B) NOG (n = 4 females) and (C-D) NSG (n = 3 females in panel C and n = 3 males in panel D) immune deficient mice intravenously exposed to ZIKV H/PF/2013 (0.5 – 1.0 x 10^6 FFU). (E) ZIKV-RNA levels in saliva of NOD/SCID (n = 4 females, green triangles), NOG (n = 4 females, blue squares) and NSG (n = 3 females, purple open circles and n = 3 males, purple closed circles) mice. (F) Kaplan-Meier plot comparing survival of ZIKV-infected BALB/c (n = 10 mice, black line) and immune deficient NOD/SCID (n = 4 mice, green line) NOG (n = 4 mice, blue line) and NSG (n = 6 mice, purple line) mice. ZIKV-RNA concentration in plasma from NSG mice intravenously exposed to ZIKV strain (G) PRVABC59 (n = 4 mice), (H) SPH2015 (n = 4 mice), and (I) BeH 819015 (n = 4 mice) (5.0 x 10^5 FFU). ZIKV-RNA was quantified by RT-PCR and the limit of detection (LOD, 833 copies per mL) is noted with a dashed line.

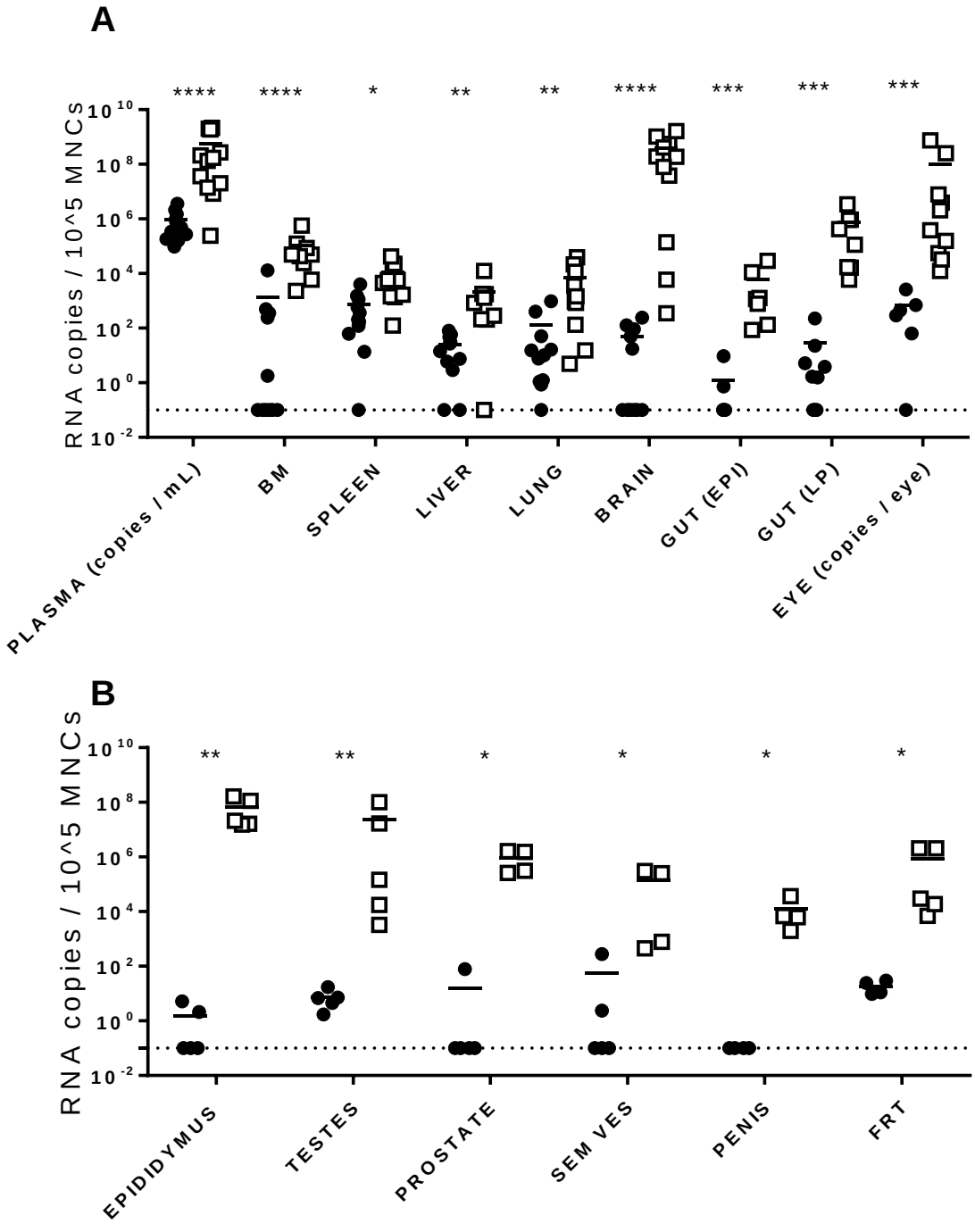

Figure 2.3. Analysis of systemic infection in immune deficient mice exposed to ZIKV. NSG mice were intravenously exposed to ZIKV H/PF/2013 (0.25 – 1 x 10^6 FFU) and tissues collected during acute or chronic infection (2 and 27-73 days post infection, respectively). RT-PCR was used to quantify ZIKV-

RNA from single cell suspensions obtained from the indicated tissues. (A) Tissues not specific to mouse gender harvested during acute (bone marrow, spleen, liver, lung, brain, n = 11; gut epithelium, gut lamina propria, n = 9, eye n = 6) or chronic (brain, lung, n = 11, eye, spleen, n = 10, bone marrow and liver, n = 9, gut epithelium, n = 7, gut lamina propria, n = 8) infection. (B) Male genital tract tissues and the female reproductive tract. Plasma and eye ZIKV-RNA levels were calculated per mL and per one whole eye, respectively. Tissues with ZIKV-RNA below the limit of detection (36 copies per 100,000 cells) are placed on the dashed line. Horizontal lines showing the mean * p=0.05, ** p = 0.01, *** p = 0.001, **** p < 0.0001, Mann-Whitney test. MNC = mononuclear cells.

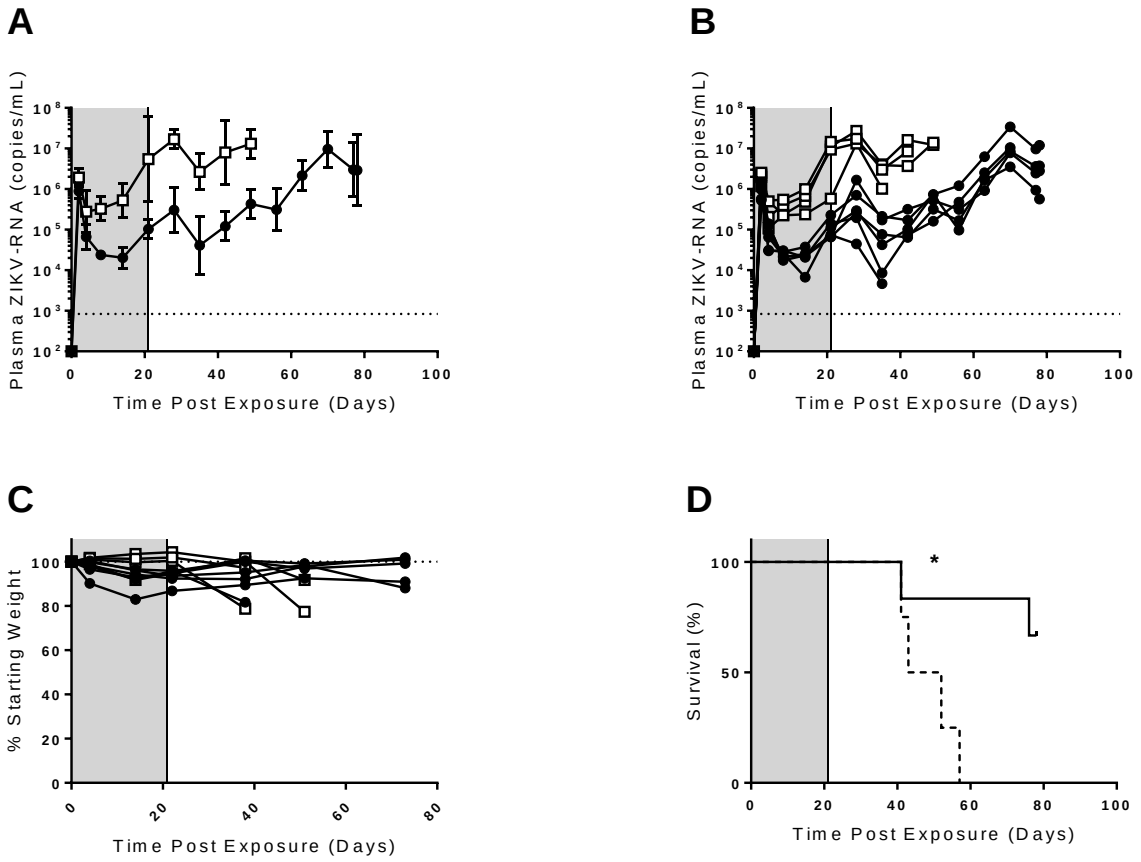

Figure 2.4. Treatment of ZIKV infected mice with DFMA reduces viremia and improves survival. (A-D) NSG mice infected with ZIKV H/PF/2013 (2.5 x 10^5 FFU) received daily DFMA (10 mg/kg, n=6 mice) or vehicle (control, n=4 mice) starting two days prior to exposure. Drug administration was continued for a total of 21 days (in grey). Plasma ZIKV-RNA levels of DFMA (black circles) and vehicle (white squares) treated mice in (A) aggregate (mean ± 95% confidence interval) or (B) individually are shown. ZIKV-RNA was quantified by RT-PCR and the limit of detection (833 copies per mL) is noted with a dashed line. ZIKV-RNA levels between DFMA-treated and control mice were compared up to 35 days post exposure using two-way repeated measures ANOVA (Treatment effect: p = 0.0001). (C) Weight of DFMA (black circles) and vehicle (white squares) treated mice following ZIKV exposure represented as percent of starting weight. (D) Kaplan-Meier plot illustrating the post-exposure survival of DFMA-treated (solid line) and control (dashed line) mice. * p = 0.05, Mantel-Cox log rank.

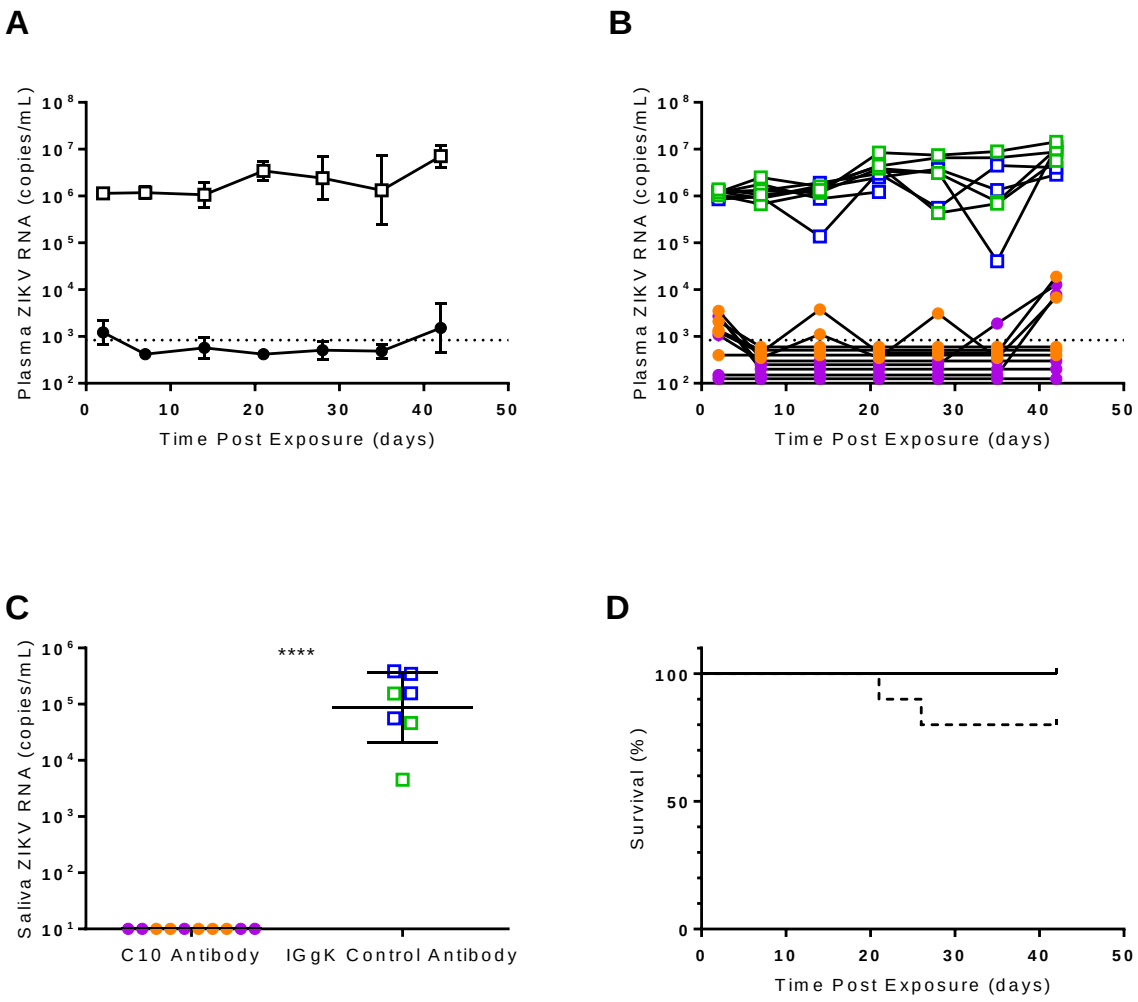

Figure 2.5. C10 neutralizing antibody administration dramatically reduces ZIKV replication and prevents viral shedding. (A) ZIKV-RNA concentration in plasma of NSG mice administered C10 neutralizing antibody intraperitoneally (62.5µg) 18 h prior to intravenous exposure to ZIKV H/PF/2013 (2.5 x 10^5 FFU) (n = 10 C10 treated mice, dark circles; n = 9 control mice, white boxes, mean ± 95% confidence interval) (B) Mice as in panel A represented individually and grouped by gender and treatment (n = 5 C10 males, purple circles, n = 5 C10 females, orange circles, n = 4 control males, blue boxes, and n = 5 control females, mice green boxes). (C) ZIKV-RNA levels in saliva collected from C10-treated (n = 10) and control mice (n = 7) 30 days post ZIKV exposure. (D) Kaplan-Meier plot illustrating the survival of C10-treated and control mice. In A-C, ZIKV-RNA was quantified by RT-PCR and the limit of detection (833 copies per mL) is shown with a dotted line. ZIKV-RNA levels between C10-treated and

control mice in panels A and B were compared using two-way repeated measures ANOVA (Treatment effect: $p<0.0001$) after exclusion of 2 mice from control group that died prematurely. Samples with ZIKV-RNA below the level of detection were assigned half the limit of detection (417 copies per mL) for statistical analysis and arbitrary values to assist with visualization in panel B. In C, a Mann-Whitney test (**** $p = 0.0001$) was used. In D, a Mantel-Cox log-rank test was used to compare survival between C10-treated and control mice.

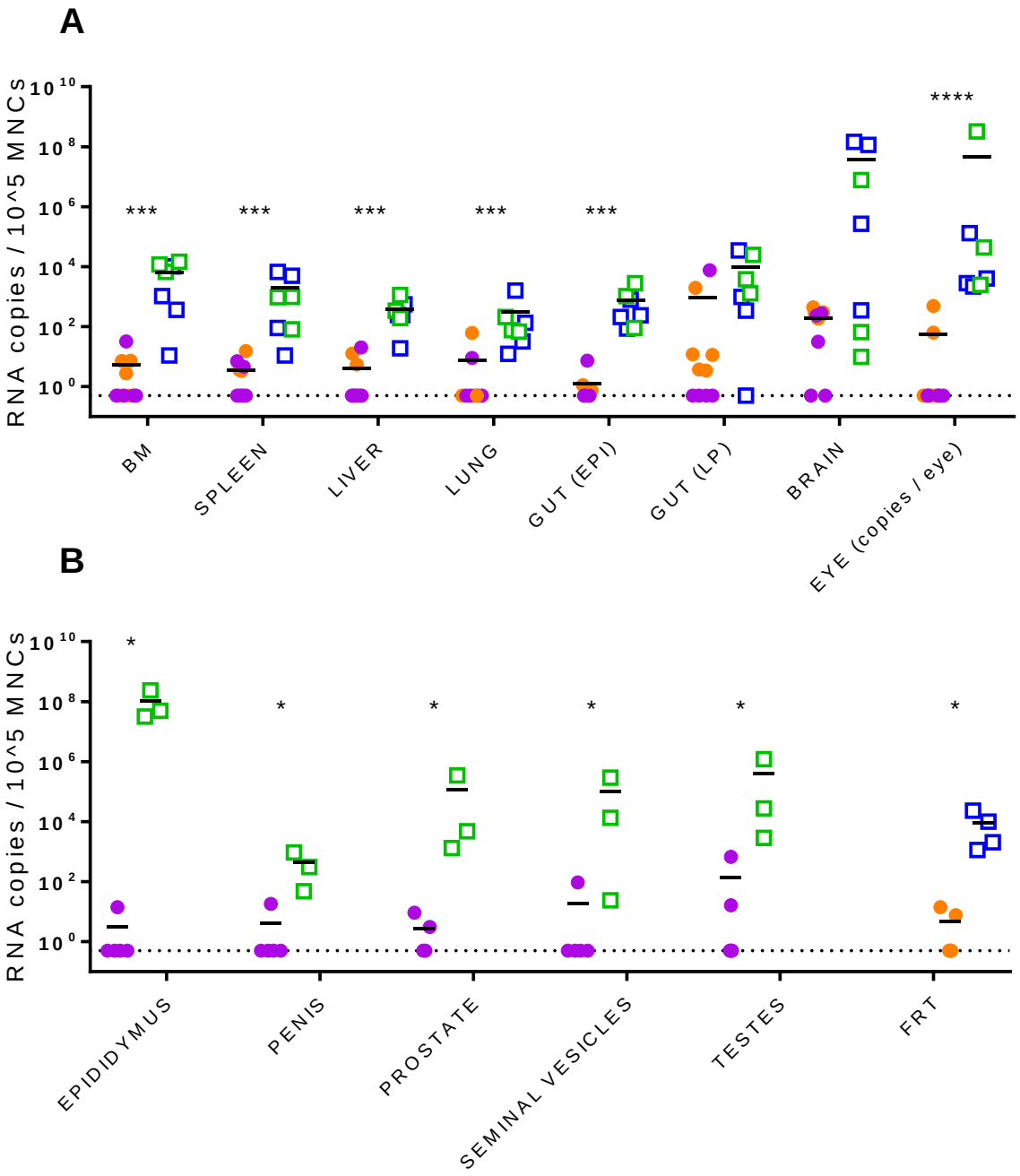

Figure 2.6. C10 antibody administration effectively reduces ZIKV replication in tissues. NSG mice were administered C10 neutralizing antibody intraperitoneally (n = 10 mice) or IgG control antibody (n = 7 mice) (62.5 µg) 18 hr prior to intravenous exposure to ZIKV H/PF/2013 (2.5 x 10^5 FFU). C10-treated male mice (n = 5) are shown in purple circles and female mice (n = 5) are shown in orange circles. Control

male mice (n = 3) are shown in green squares and control female mice (n = 4) are shown in blue squares. RT-PCR was used to quantify ZIKV-RNA levels in mononuclear cell suspensions of tissues collected 42-44 days post exposure. ZIKV-RNA concentration in (A) tissues not specific to mouse gender and (B) tissues from the male genital tract and female reproductive tract. RNA measurements below the limit of detection are shown on the dotted line. Horizontal lines showing the mean, * $p = 0.05$, ** $p = 0.01$, *** $p = 0.001$, **** $p < 0.0001$, Mann-Whitney test. MNC = mononuclear cells.

Supplemental information

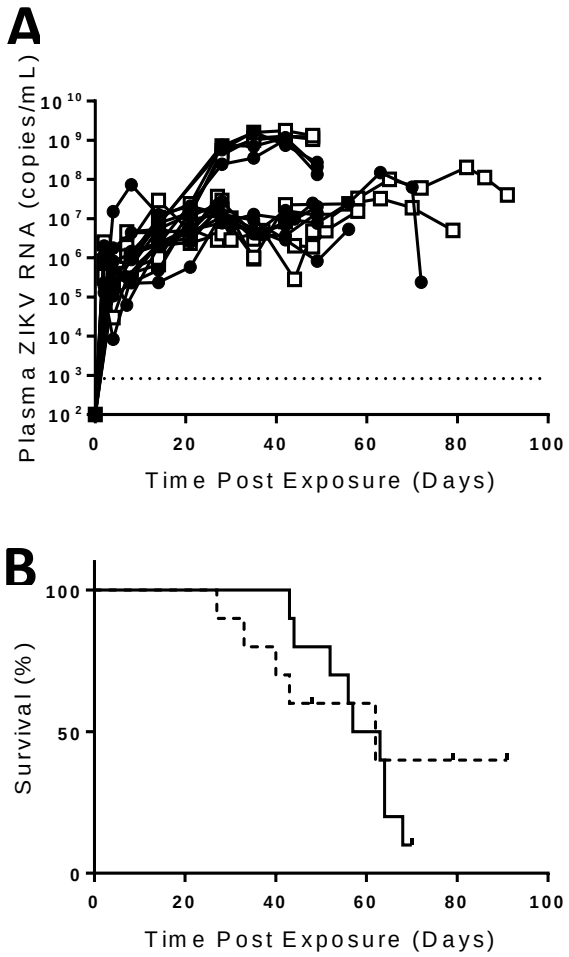

Supplementary Figure 2.1. Male and female mice were similar in mean levels of peripheral ZIKV-RNA and survival. NSG mice (10 male, 10 female) were intravenously exposed to FFU ZIKV H/PF/2013 (0.25 – 1 x 10^6). (A) Longitudinal monitoring of plasma viral load quantified by RT-PCR. Legend: the lower limit of detection (dotted line, 833 copies/mL of plasma), males (black dots) and females (white dots). (B) Kaplan-Meier curves for post-exposure survival of the males and females were similar. The logrank test of the null hypothesis "the gender effect is exactly zero" was inconclusive ($p = 0.8317$) and the proportional hazards assumption was not met.

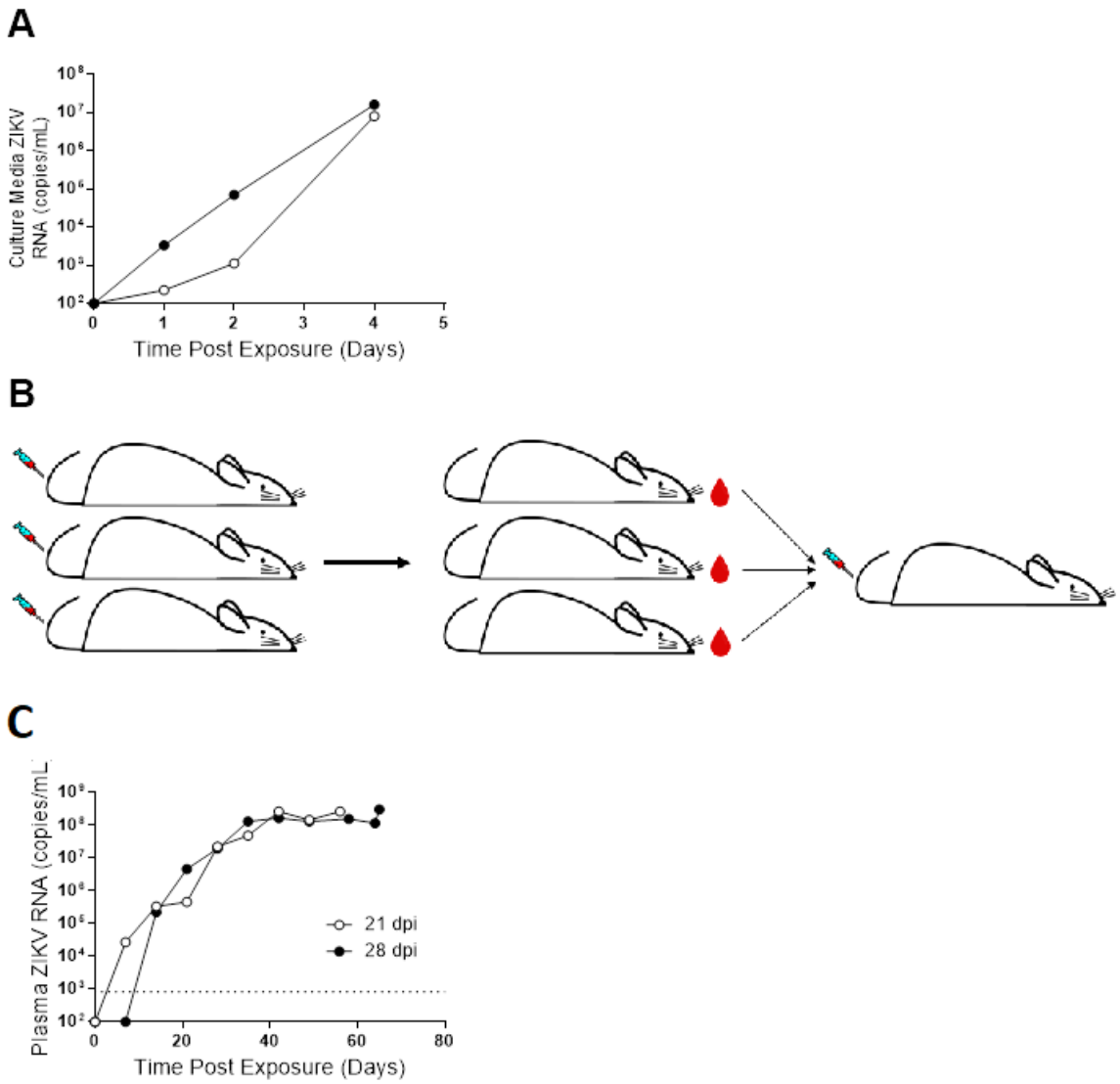

Supplementary Figure 2.2. ZIKV isolated from infected mice efficiently replicates both *in vitro* and *in vivo*. (A) Serum (3µL) from infected mice was used to inoculate VERO cells. ZIKV-RNA was then quantified in culture media by RT-PCR at the indicated time points. (B) Experimental design. Three mice were exposed intravenously to ZIKV H/PF/2013. After 21 days, 20 µL serum from each mouse was pooled before intravenous inoculation into a female naïve mouse. This process was repeated in a male naïve mouse with serum collected from infected mice 28 days after exposure. Plasma from exposed mice was then monitored for the presence of ZIKV-RNA at the indicated time points (C). The limit of detection (833 copies/mL plasma) is indicated by a dotted line.

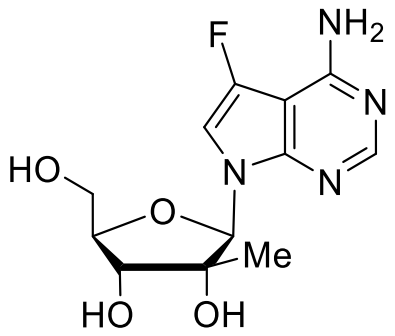

Supplementary Figure 2.3. Chemical structure of DFMA.

Supplementary Table 2.1. ZIKV-RNA is shed into the urine and CVL of infected mice.

Weeks[#]	CVL[*]	Proportion	Lower[a]	Upper[b]	Urine	Proportion	Lower[a]	Upper[b]
2	--	--	--	--	0/1	0.00	0.00	0.79
3	2/3	0.67	0.21	0.94	2/2	1.00	0.34	1.00
5	3/3	1.00	0.44	1.00	1/1	1.00	0.21	1.00
6	3/3	1.00	0.44	1.00	1/2	0.50	0.09	0.91
8	1/1	1.00	0.21	1.00	1/1	1.00	0.21	1.00
9	--	--	--	--	0/3	0.00	0.00	0.56

[#]Bodily secretions were sampled from infected mice at the indicated weeks post infection and ZIKV-RNA was analyzed by RT-PCR.

Results are represented as positive samples from total mice sampled.

-- indicates samples not analyzed.

*CVL, cervicovaginal secretions.

a. Lower 95% confidence limit

b. Upper 95% confidence limit

Methods

Mice

Immunodeficient NOD/SCID/$\gamma c^{-/-}$ (NSG) mice, NOD/SCID (The Jackson Laboratory, Bar Harbor, ME), and NOG (Taconic Biosciences, Rensselaer, NY) male and female mice were used for experiments at 12-20 weeks of age. Mice were maintained by the Division of Comparative Medicine at UNC-Chapel Hill according to protocol approved by the Institutional Animal Care and Use Committee.

Virus challenges and administration of DFMA and C10 antibody

Stocks of ZIKV H/PF/2013, SPH2015, PRVABC59, and BeH819015 were prepared as previously described (50). Viral challenges were performed by diluting viral stocks in RPMI (Gibco, Gaithersburg, MD). Virus (0.25-1.0 x 10^6 FFU) was administered intravenously via tail vein injection (200 µL volume). C10 antibody (62.5 µg) was diluted in saline (Hospira, Lake Forest, IL) and administered systemically via intraperitoneal injection (200 µL volume) 18 hr prior to viral challenge. Monoclonal antibody C10 was prepared using transfected human 293T cells from cloned plasmids as previously described (50). DFMA was prepared by direct chemical synthesis and its structure confirmed by mass spectrometry and proton NMR (synthesis to be published elsewhere). DFMA was dissolved in DMSO (Fisher Scientific, Hampton, NC) and diluted in PBS (Sigma-Aldrich, St. Louis, MO) before filtration with a 70 µm syringe filter (Corning, NY) and systemic administered via intraperitoneal injection.

Collection and processing of mouse bodily fluids

Mouse peripheral blood and bodily secretions were collected longitudinally for ZIKV-RNA quantification. Peripheral blood was collected into tubes containing anti-coagulant (EDTA solution, Sigma-Aldrich, St. Louis, MD). Plasma was separated by centrifugation. To stimulate salivation, ZIKV-infected mice were administered pilocarpine HCl (Sigma-Aldrich, St. Louis, MD) in sterile PBS (100 µg/100 µL) by intraperitoneal injection essentially as previously described (51). Saliva was collected directly from the mouth with a micropipette. Cervicovaginal secretions were obtained by cervicovaginal lavage with 3 successive washes of 20 µL sterile PBS using sterile filter micropipette tips inserted less than 3 mm into the vaginal canal. Urine was collected by holding mice above a sterile petri dish and lightly palpating above the bladder to induce urination. The urine was then collected from the petri dish. Cells and debris from bodily fluids were removed by centrifugation.

Collection and processing of tissues

Mouse tissues were collected essentially as previously described (52-55). Tissues collected for analysis (depending on mouse gender) included the spleen, bone marrow, lungs, liver, gastrointestinal tract, brain, eyes, FRT, epididymis, testes, prostate, penis, and seminal vesicles. For ZIKV-RNA analysis, tissues were processed into single cell suspensions as previously described (52-55). In brief, cells were isolated by forcing tissues through a 70 µm cell strainer (Falcon, Corning, NY) followed by red blood cell lysis if necessary. The liver, lung, female reproductive tract, and penis were digested in an enzyme digest cocktail prior to filtration. Liver, lung, and brain cells were purified with percoll gradients (GE Healthcare, Little Chalfont, UK). The mouse gastrointestinal tract was flushed with PBS and incubated with a dithiothreitol (Fisher Scientific, Hampton, NC) and EDTA solution to isolate cells from the intraepithelial layer and incubated with elastase (Worthington Biochemical, Lakewood, NJ) and hyaluronidase (Worthington Biochemical, NJ) to isolate the cells from the lamina propria layer (55).

ZIKV-RNA analysis

RNA was extracted from plasma (40 µL) using the QIAmp Viral RNA kit (Qiagen). Tissue RNA was extracted using RNeasy mini columns (Qiagen) according to the manufacture's protocol including an optional treatment with RNase-free DNase. ZIKV-RNA levels in the peripheral blood plasma from infected mice were measured using a one-step quantitative real-time PCR (TaqMan® RNA to-CT 1-step kit, Applied Biosystems, Foster City, CA). The sequences of the forward and reverse primers and the TaqMan® probe for PCR amplification and detection of ZIKV RNA were: 5′-CCGCTGCCCAACACAAG -3′, 5′-CCACTAACGTTCTTTTGCAGACAT -3′, and 5′-FAM-AGCCTACCT/ZEN/TGACAAGCAGTCAGACACACTCAA-Q-3′, respectively (3). ZIKV-RNA was transcribed using a custom synthesized plasmid (Biomatik) to create a standard curve. Sample RNA was quantified by interpolation from the standard curve. All samples were run and analyzed on an ABI 7500 Fast Real Time PCR System (Applied Biosystems, Foster City, CA).

Statistical Analysis

If not otherwise specified, sample means are reported along with the corresponding standard error (s.e.m.) which conveys information about the level of imprecision.

The estimators and statistical test procedures used in this study are described in the figure legends and in the narrative text in the results section. For example, the DFMA treatment and the control treatment were compared in terms of longitudinal measures of ZIKV-RNA copies/mL. The analysis relied on a two-way repeated measures ANOVA model in which the fixed effects represented time and treatment regimen. The model did not include time-by-treatment interaction terms. The null hypothesis "the DFMA treatment effect is exactly zero" was tested using an F-test procedure. The same approach was used in the analysis of the relative efficacy of C10.

To ensure appropriate blinding, the investigators involved in analyzing tissue samples for viral loads were given numbered samples, and were thus unable to know treatment group identity (treated, controls). No other blinding procedures were used in the study. No statistical methods were used to pre-determined sample size. No randomization was not used to allocate animals/samples to experimental groups or to the various stages of the study.

All statistical computations were performed using GraphPad Prism (version 6.0 for Mac, GraphPad Software, La Jolla, California).

REFERENCES

1. Musso D, Gubler DJ. 2016. Zika Virus. Clin Microbiol Rev 29:487-524.

2. Duffy MR, Chen TH, Hancock WT, Powers AM, Kool JL, Lanciotti RS, Pretrick M, Marfel M, Holzbauer S, Dubray C, Guillaumot L, Griggs A, Bel M, Lambert AJ, Laven J, Kosoy O, Panella A, Biggerstaff BJ, Fischer M, Hayes EB. 2009. Zika virus outbreak on Yap Island, Federated States of Micronesia. N Engl J Med 360:2536-43.

3. Lanciotti RS, Kosoy OL, Laven JJ, Velez JO, Lambert AJ, Johnson AJ, Stanfield SM, Duffy MR. 2008. Genetic and serologic properties of Zika virus associated with an epidemic, Yap State, Micronesia, 2007. Emerg Infect Dis 14:1232-9.

4. Aubry M, Teissier A, Huart M, Merceron S, Vanhomwegen J, Roche C, Vial AL, Teururai S, Sicard S, Paulous S, Despres P, Manuguerra JC, Mallet HP, Musso D, Deparis X, Cao-Lormeau VM. 2017. Zika Virus Seroprevalence, French Polynesia, 2014-2015. Emerg Infect Dis 23:669-672.

5. Cao-Lormeau VM, Blake A, Mons S, Lastere S, Roche C, Vanhomwegen J, Dub T, Baudouin L, Teissier A, Larre P, Vial AL, Decam C, Choumet V, Halstead SK, Willison HJ, Musset L, Manuguerra JC, Despres P, Fournier E, Mallet HP, Musso D, Fontanet A, Neil J, Ghawche F. 2016. Guillain-Barre Syndrome outbreak associated with Zika virus infection in French Polynesia: a case-control study. Lancet 387:1531-1539.

6. Hennessey M, Fischer M, Staples JE. 2016. Zika Virus Spreads to New Areas - Region of the Americas, May 2015-January 2016. MMWR Morb Mortal Wkly Rep 65:55-8.

7. Mlakar J, Korva M, Tul N, Popovic M, Poljsak-Prijatelj M, Mraz J, Kolenc M, Resman Rus K, Vesnaver Vipotnik T, Fabjan Vodusek V, Vizjak A, Pizem J, Petrovec M, Avsic Zupanc T. 2016. Zika Virus Associated with Microcephaly. N Engl J Med 374:951-8.

8. Schuler-Faccini L, Ribeiro EM, Feitosa IM, Horovitz DD, Cavalcanti DP, Pessoa A, Doriqui MJ, Neri JI, Neto JM, Wanderley HY, Cernach M, El-Husny AS, Pone MV, Serao CL, Sanseverino MT. 2016. Possible Association Between Zika Virus Infection and Microcephaly - Brazil, 2015. MMWR Morb Mortal Wkly Rep 65:59-62.

9. de Paula Freitas B, Ventura CV, Maia M, Belfort R, Jr. 2017. Zika virus and the eye. Curr Opin Ophthalmol 28:595-599.

10. Hamer DH, Wilson ME, Jean J, Chen LH. 2017. Epidemiology, Prevention, and Potential Future Treatments of Sexually Transmitted Zika Virus Infection. Curr Infect Dis Rep 19:16.

11. D'Ortenzio E, Matheron S, Yazdanpanah Y, de Lamballerie X, Hubert B, Piorkowski G, Maquart M, Descamps D, Damond F, Leparc-Goffart I. 2016. Evidence of Sexual Transmission of Zika Virus. N Engl J Med 374:2195-8.

12. Mead PS, Duggal NK, Hook SA, Delorey M, Fischer M, Olzenak McGuire D, Becksted H, Max RJ, Anishchenko M, Schwartz AM, Tzeng WP, Nelson CA, McDonald EM, Brooks JT, Brault AC, Hinckley AF. 2018. Zika Virus Shedding in Semen of Symptomatic Infected Men. N Engl J Med 378:1377-1385.

13. Krow-Lucal ER, Novosad SA, Dunn AC, Brent CR, Savage HM, Faraji A, Peterson D, Dibbs A, Vietor B, Christensen K, Laven JJ, Godsey MS, Jr., Christensen B, Beyer B, Cortese MM, Johnson NC, Panella AJ, Biggerstaff BJ, Rubin M, Fridkin SK, Staples JE, Nakashima AK. 2017. Zika Virus Infection in Patient with No Known Risk Factors, Utah, USA, 2016. Emerg Infect Dis 23:1260-1267.

14. Aid M, Abbink P, Larocca RA, Boyd M, Nityanandam R, Nanayakkara O, Martinot AJ, Moseley ET, Blass E, Borducchi EN, Chandrashekar A, Brinkman AL, Molloy K, Jetton D, Tartaglia LJ, Liu J, Best K, Perelson AS, De La Barrera RA, Lewis MG, Barouch DH. 2017. Zika Virus Persistence in the Central Nervous System and Lymph Nodes of Rhesus Monkeys. Cell 169:610-620.e14.

15. Larocca RA, Abbink P, Peron JPS, de AZPM, Iampietro MJ, Badamchi-Zadeh A, Boyd M, Ng'ang'a D, Kirilova M, Nityanandam R, Mercado NB, Li Z, Moseley ET, Bricault CA, Borducchi EN, Giglio PB, Jetton D, Neubauer G, Nkolola JP, Maxfield LF, De La Barrera RA, Jarman RG, Eckels KH, Michael NL, Thomas SJ, Barouch DH. 2016. Vaccine Protection Against Zika Virus from Brazil. Nature 536:474-8.

16. Lazear HM, Govero J, Smith AM, Platt DJ, Fernandez E, Miner JJ, Diamond MS. 2016. A Mouse Model of Zika Virus Pathogenesis. Cell Host Microbe 19:720-30.

17. Rossi SL, Tesh RB, Azar SR, Muruato AE, Hanley KA, Auguste AJ, Langsjoen RM, Paessler S, Vasilakis N, Weaver SC. 2016. Characterization of a Novel Murine Model to Study Zika Virus. Am J Trop Med Hyg 94:1362-9.

18. Grant A, Ponia SS, Tripathi S, Balasubramaniam V, Miorin L, Sourisseau M, Schwarz MC, Sanchez-Seco MP, Evans MJ, Best SM, Garcia-Sastre A. 2016. Zika Virus Targets Human STAT2 to Inhibit Type I Interferon Signaling. Cell Host Microbe 19:882-90.

19. Kumar A, Hou S, Airo AM, Limonta D, Mancinelli V, Branton W, Power C, Hobman TC. 2016. Zika virus inhibits type-I interferon production and downstream signaling. EMBO Rep 17:1766-1775.

20. Tripathi S, Balasubramaniam VR, Brown JA, Mena I, Grant A, Bardina SV, Maringer K, Schwarz MC, Maestre AM, Sourisseau M, Albrecht RA, Krammer F, Evans MJ, Fernandez-Sesma A, Lim JK, Garcia-Sastre A. 2017. A novel Zika virus mouse model reveals strain specific differences in virus pathogenesis and host inflammatory immune responses. PLoS Pathog 13:e1006258.

21. Dowall SD, Graham VA, Rayner E, Atkinson B, Hall G, Watson RJ, Bosworth A, Bonney LC, Kitchen S, Hewson R. 2016. A Susceptible Mouse Model for Zika Virus Infection. PLoS Negl Trop Dis 10:e0004658.

22. Winkler CW, Myers LM, Woods TA, Messer RJ, Carmody AB, McNally KL, Scott DP, Hasenkrug KJ, Best SM, Peterson KE. 2017. Adaptive Immune Responses to Zika Virus Are Important for Controlling Virus Infection and Preventing Infection in Brain and Testes. J Immunol 198:3526-3535.

23. Aliota MT, Caine EA, Walker EC, Larkin KE, Camacho E, Osorio JE. 2016. Characterization of Lethal Zika Virus Infection in AG129 Mice. PLoS Negl Trop Dis 10:e0004682.

24. Miner JJ, Sene A, Richner JM, Smith AM, Santeford A, Ban N, Weger-Lucarelli J, Manzella F, Ruckert C, Govero J, Noguchi KK, Ebel GD, Diamond MS, Apte RS. 2016. Zika Virus Infection in Mice Causes Panuveitis with Shedding of Virus in Tears. Cell Rep 16:3208-3218.

25. Julander JG, Siddharthan V, Evans J, Taylor R, Tolbert K, Apuli C, Stewart J, Collins P, Gebre M, Neilson S, Van Wettere A, Lee YM, Sheridan WP, Morrey JD, Babu YS. 2017. Efficacy of the broad-spectrum antiviral compound BCX4430 against Zika virus in cell culture and in a mouse model. Antiviral Res 137:14-22.

26. Sumathy K, Kulkarni B, Gondu RK, Ponnuru SK, Bonguram N, Eligeti R, Gadiyaram S, Praturi U, Chougule B, Karunakaran L, Ella KM. 2017. Protective efficacy of Zika vaccine in AG129 mouse model. Sci Rep 7:46375.

27. Duggal NK, Ritter JM, Pestorius SE, Zaki SR, Davis BS, Chang GJ, Bowen RA, Brault AC. 2017. Frequent Zika Virus Sexual Transmission and Prolonged Viral RNA Shedding in an Immunodeficient Mouse Model. Cell Rep 18:1751-1760.

28. Smith DR, Hollidge B, Daye S, Zeng X, Blancett C, Kuszpit K, Bocan T, Koehler JW, Coyne S, Minogue T, Kenny T, Chi X, Yim S, Miller L, Schmaljohn C, Bavari S, Golden JW. 2017. Neuropathogenesis of Zika Virus in a Highly Susceptible Immunocompetent Mouse Model after Antibody Blockade of Type I Interferon. PLoS Negl Trop Dis 11:e0005296.

29. Chan JF, Zhang AJ, Chan CC, Yip CC, Mak WW, Zhu H, Poon VK, Tee KM, Zhu Z, Cai JP, Tsang JO, Chik KK, Yin F, Chan KH, Kok KH, Jin DY, Au-Yeung RK, Yuen KY. 2016. Zika Virus Infection in Dexamethasone-immunosuppressed Mice Demonstrating Disseminated Infection with Multi-organ Involvement Including Orchitis Effectively Treated by Recombinant Type I Interferons. EBioMedicine 14:112-122.

30. Winkler CW, Woods TA, Rosenke R, Scott DP, Best SM, Peterson KE. 2017. Sexual and Vertical Transmission of Zika Virus in anti-interferon receptor-treated Rag1-deficient mice. Sci Rep 7:7176.

31. Bonaldo MC, Ribeiro IP, Lima NS, Dos Santos AA, Menezes LS, da Cruz SO, de Mello IS, Furtado ND, de Moura EE, Damasceno L, da Silva KA, de Castro MG, Gerber AL, de Almeida LG, Lourenco-de-Oliveira R, Vasconcelos AT, Brasil P. 2016. Isolation of Infective Zika Virus from Urine and Saliva of Patients in Brazil. PLoS Negl Trop Dis 10:e0004816.

32. Colt S, Garcia-Casal MN, Pena-Rosas JP, Finkelstein JL, Rayco-Solon P, Weise Prinzo ZC, Mehta S. 2017. Transmission of Zika virus through breast milk and other breastfeeding-related bodily-fluids: A systematic review. PLoS Negl Trop Dis 11:e0005528.

33. Iannetta M, Lalle E, Musso M, Carletti F, Scorzolini L, D'Abramo A, Chinello P, Castilletti C, Ippolito G, Capobianchi MR, Nicastri E. 2017. Persistent detection of dengue virus RNA in vaginal secretion of a woman returning from Sri Lanka to Italy, April 2017. Euro Surveill 22.

34. Joguet G, Mansuy JM, Matusali G, Hamdi S, Walschaerts M, Pavili L, Guyomard S, Prisant N, Lamarre P, Dejucq-Rainsford N, Pasquier C, Bujan L. 2017. Effect of acute Zika virus infection on sperm and virus clearance in body fluids: a prospective observational study. Lancet Infect Dis 17:1200-1208.

35. Zmurko J, Marques RE, Schols D, Verbeken E, Kaptein SJ, Neyts J. 2016. The Viral Polymerase Inhibitor 7-Deaza-2'-C-Methyladenosine Is a Potent Inhibitor of In Vitro Zika Virus Replication and Delays Disease Progression in a Robust Mouse Infection Model. PLoS Negl Trop Dis 10:e0004695.

36. Swanstrom JA, Plante JA, Plante KS, Young EF, McGowan E, Gallichotte EN, Widman DG, Heise MT, de Silva AM, Baric RS. 2016. Dengue Virus Envelope Dimer Epitope Monoclonal Antibodies Isolated from Dengue Patients Are Protective against Zika Virus. MBio 7.

37. Miner JJ, Diamond MS. 2017. Zika virus pathogenesis and tissue tropism. Cell Host Microbe 21:134-42.

38. Yepez JB, Murati FA, Pettito M, Penaranda CF, de Yepez J, Maestre G, Arevalo JF. 2017. Ophthalmic Manifestations of Congenital Zika Syndrome in Colombia and Venezuela. JAMA Ophthalmol 135:440-445.

39. Manangeeswaran M, Kielczewski JL, Sen HN, Xu BC, Ireland DDC, McWilliams IL, Chan CC, Caspi RR, Verthelyi D. 2018. ZIKA virus infection causes persistent chorioretinal lesions. Emerg Microbes Infect 7:96.

40. Furtado JM, Esposito DL, Klein TM, Teixeira-Pinto T, da Fonseca BA. 2016. Uveitis Associated with Zika Virus Infection. N Engl J Med 375:394-6.

41. Zhao Z, Yang M, Azar SR, Soong L, Weaver SC, Sun J, Chen Y, Rossi SL, Cai J. 2017. Viral Retinopathy in Experimental Models of Zika Infection. Invest Ophthalmol Vis Sci 58:4355-4365.

42. Zhang S, Kostyuchenko VA, Ng TS, Lim XN, Ooi JS, Lambert S, Tan TY, Widman DG, Shi J, Baric RS, Lok SM. 2016. Neutralization mechanism of a highly potent antibody against Zika virus. Nat Commun 7:13679.

43. Azevedo RS, Araujo MT, Martins Filho AJ, Oliveira CS, Nunes BT, Cruz AC, Nascimento AG, Medeiros RC, Caldas CA, Araujo FC, Quaresma JA, Vasconcelos BC, Queiroz MG, da Rosa ES, Henriques DF, Silva EV, Chiang JO, Martins LC, Medeiros DB, Lima JA, Nunes MR, Cardoso JF, Silva SP, Shi PY, Tesh RB, Rodrigues SG, Vasconcelos PF. 2016. Zika virus epidemic in Brazil. I. Fatal disease in adults: Clinical and laboratorial aspects. J Clin Virol 85:56-64.

44. Xu M, Lee EM, Wen Z, Cheng Y, Huang WK, Qian X, Tcw J, Kouznetsova J, Ogden SC, Hammack C, Jacob F, Nguyen HN, Itkin M, Hanna C, Shinn P, Allen C, Michael SG, Simeonov A, Huang W, Christian KM, Goate A, Brennand KJ, Huang R, Xia M, Ming GL, Zheng W, Song H, Tang H. 2016. Identification of small-molecule inhibitors of Zika virus infection and induced neural cell death via a drug repurposing screen. Nat Med 22:1101-1107.

45. Barrows NJ, Campos RK, Powell ST, Prasanth KR, Schott-Lerner G, Soto-Acosta R, Galarza-Munoz G, McGrath EL, Urrabaz-Garza R, Gao J, Wu P, Menon R, Saade G, Fernandez-Salas I, Rossi SL, Vasilakis N, Routh A, Bradrick SS, Garcia-Blanco MA. 2016. A Screen of FDA-Approved Drugs for Inhibitors of Zika Virus Infection. Cell Host Microbe 20:259-70.

46. Bullard-Feibelman KM, Govero J, Zhu Z, Salazar V, Veselinovic M, Diamond MS, Geiss BJ. 2017. The FDA-approved drug sofosbuvir inhibits Zika virus infection. Antiviral Res 137:134-140.

47. Sacramento CQ, de Melo GR, de Freitas CS, Rocha N, Hoelz LV, Miranda M, Fintelman-Rodrigues N, Marttorelli A, Ferreira AC, Barbosa-Lima G, Abrantes JL, Vieira YR, Bastos MM, de Mello Volotao E, Nunes EP, Tschoeke DA, Leomil L, Loiola EC, Trindade P, Rehen SK, Bozza FA, Bozza PT, Boechat N, Thompson FL, de Filippis AM, Bruning K, Souza TM. 2017. The clinically approved antiviral drug sofosbuvir inhibits Zika virus replication. Sci Rep 7:40920.

48. Mesci P, Macia A, Moore SM, Shiryaev SA, Pinto A, Huang CT, Tejwani L, Fernandes IR, Suarez NA, Kolar MJ, Montefusco S, Rosenberg SC, Herai RH, Cugola FR, Russo FB, Sheets N, Saghatelian A, Shresta S, Momper JD, Siqueira-Neto JL, Corbett KD, Beltrao-Braga PCB, Terskikh AV, Muotri AR. 2018. Blocking Zika virus vertical transmission. Sci Rep 8:1218.

49. Ferreira AC, Zaverucha-do-Valle C, Reis PA, Barbosa-Lima G, Vieira YR, Mattos M, Silva PP, Sacramento C, de Castro Faria Neto HC, Campanati L, Tanuri A, Bruning K, Bozza FA, Bozza PT, Souza TML. 2017. Sofosbuvir protects Zika virus-infected mice from mortality, preventing short- and long-term sequelae. Sci Rep 7:9409.

50. Zhang S, Kostyuchenko VA, Ng TS, Lim XN, Ooi JSG, Lambert S, Tan TY, Widman DG, Shi J, Baric RS, Lok SM. 2016. Neutralization mechanism of a highly potent antibody against Zika virus. Nat Commun 7.

51. Kovarova M, Shanmugasundaram U, Baker CE, Spagnuolo RA, De C, Nixon CC, Wahl A, Garcia JV. 2016. HIV pre-exposure prophylaxis for women and infants prevents vaginal and oral HIV transmission in a preclinical model of HIV infection. J Antimicrob Chemother 71:3185-3194.

52. Denton PW, Estes JD, Sun Z, Othieno FA, Wei BL, Wege AK, Powell DA, Payne D, Haase AT, Garcia JV. 2008. Antiretroviral pre-exposure prophylaxis prevents vaginal transmission of HIV-1 in humanized BLT mice. PLoS Med 5:e16.

53. Olesen R, Wahl A, Denton PW, Garcia JV. 2011. Immune reconstitution of the female reproductive tract of humanized BLT mice and their susceptibility to human immunodeficiency virus infection. J Reprod Immunol 88:195-203.

54. Denton PW, Nochi T, Lim A, Krisko JF, Martinez-Torres F, Choudhary SK, Wahl A, Olesen R, Zou W, Di Santo JP, Margolis DM, Garcia JV. 2012. IL-2 receptor gamma-chain molecule is critical for intestinal T-cell reconstitution in humanized mice. Mucosal Immunol 5:555-66.

55. Shanmugasundaram U, Kovarova M, Ho PT, Schramm N, Wahl A, Parniak MA, Garcia JV. 2016. Efficient Inhibition of HIV Replication in the Gastrointestinal and Female Reproductive Tracts of Humanized BLT Mice by EFdA. PLoS One 11:e0159517.